

Routh Reduction for Flyball Governors

Thomas Coppin

Supervised by Dr Jochen Trumpf

ENGN4712

2015

Acknowledgements

I would like to thank my supervisor, Dr. Jochen Trumpf, for providing help and support with the project throughout the year.

Abstract

This paper investigates the application of Routh reduction to a Watt flyball governor. The method is used to derive a dynamic model of both the governor on its own, and a joint engine-governor system, finding that, in this case, applying Routh reduction either before or after combining the engine and governor gives the same result. Using this method, it was determined that the dynamic model for the governor takes the form of a damped harmonic oscillator. The paper then moves on to examine the stability of both the governor on its own, and the joint engine-governor system, and concludes that the governor is always stable, whilst there is a relationship between the governor parameters, the engine parameters, and the operating point that determines whether or not the joint system is stable. Lastly, the transient step response of the joint model was analysed and used to define a PID controller capable of performing the same control action as the linear part of the governor. This controller was purely integral, and the governor was found to apply both an integral control action and a frictional force to the engine. Additionally, a brief outline of Watt governor design is provided throughout, focussing on how the governor parameters affect the velocity profile and the transient response of the system.

Contents

Acknowledgments	i
Abstract	ii
1 Aim	1
2 Introduction	2
2.1 Flyball Governors	2
2.1.1 The Watt Governor	3
2.1.2 The Porter Governor	4
2.1.3 The Proell Governor	5
2.1.4 The Hartnell Governor	6
2.2 Stability	6
2.2.1 Routh Stability	7
2.2.2 Maxwell Stability	7
2.3 Digital Feedback Control Mechanisms	8
2.3.1 Feedback	8
2.3.2 PID Controllers	8
3 A Dynamic Model for a Watt Engine-Governor System	9
3.1 Dynamic Model for the Watt Governor	9
3.1.1 Generalised Forces	11
3.1.2 Lagrangian	13
3.1.3 Routh Reduction	19
3.2 Dynamic Model for the Joint System	21
3.2.1 Dynamic Model for the Engine	21
3.2.2 Combining the Models	21

3.2.3	Alternative Joint Model Derivation	22
3.3	Watt Governor Design	25
3.3.1	Validation of Negligible Rod Mass Assumption	25
3.3.2	Effect of Governor Parameters	26
4	Stability Analysis	29
4.1	Routh Stability	29
4.2	Maxwell Stability	33
4.2.1	Linearisation	33
4.2.2	Stability	34
4.3	Transient Response	35
5	A Similar Digital Feedback Controller	40
5.1	Joint System Transfer Function	40
5.1.1	Further Governor Design	42
5.2	PID Controller	44
5.2.1	Transfer Function Derivation	44
5.2.2	Comparison with Governor	47
6	Conclusion	49
6.1	Further Work	49
A	Appendices	52
A.1	Variables in their Expanded Forms	52
A.2	Governor Design	53
A.3	Matlab Code	57

List of Figures

2.1	Watt Governor	3
2.2	Porter Governor	4
2.3	Proell Governor	5
2.4	Hartnell Governor	6
3.1	Image Showing Choice of Coordinates for Euler-Lagrange Formalism	10
3.2	Image Showing Parameters used during derivation of equation of motion	11
3.3	Image Showing Choice of Frames for Parallel Axis Theorem	13
3.4	Image Showing Choice of Parameters Used for Calculating Potential Term	17
3.5	Engine Diagram	23
3.6	Velocity Profile - Changing Rod Mass	26
3.7	Velocity Profile - Changing Governor Arm Length	27
3.8	Velocity Graph - Changing Governor Arm Length	28
4.1	Plot of the LHS of Equation (4.4)	32
4.2	Plot of Stability Simulation for Watt Governor	32
4.3	Input Step Function ' τ '	36
4.4	Governor Angle Transient Response	37
4.5	Engine Speed Transient Response	37
4.6	Governor Angle Transient Response - Increased Friction Coefficient	38
4.7	Engine Speed Transient Response - Increased Friction Coefficient	39
5.1	Annotated Engine Speed Transient Response Plot	41
5.2	Digital Feedback Controller Block Diagram	44
5.3	Engine Speed Transient Response using Governor Model (left) and PID Controller Model (right)	48

§0.0. LIST OF FIGURES

A.1	Velocity Profile - Changing Governor Arm Extension	53
A.2	Velocity Profile - Changing Flyball Radius	54
A.3	Velocity Graph - Changing Governor Arm Extension	54
A.4	Velocity Graph - Changing Flyball Radius	55
A.5	Velocity Profile - Combining $2^*a'$ and $2^*b'$	55
A.6	Velocity Profile - Combining $2^*a'$ and $1/2^*b'$	56
A.7	Velocity Profile - Combining $1/2^*a'$ and $1/2^*b'$	56
A.8	Velocity Graph - Changing 'a' & 'b'	57
A.9	Simulink Model used to simulate Transient Response of PID Controlled Feed-back Loop	65

Aim

This paper had three main aims, they were:

- To derive a dynamic model for a Watt flyball governor, and a joint steam engine-governor system, that is capable of accurately modelling its behaviour;
- To examine the stability of both the governor on its own, and the joint engine-governor system, and possibly develop a set of criteria that determine this, and;
- To develop a PID controller that is capable of performing the same control action on the engine as the governor.

Introduction

2.1 Flyball Governors

Flyball governors are centrifugal governors that are used to control the rotational speed of engines by controlling the amount of working fluid that reaches the engine. They have been used from as early as the 17th century to control the speed of millstones in windmills, but rose to popularity after being employed by James Watt in steam engines [1]. Flyball governors are still in use today, being installed in many modern turbines or some internal combustion engines. Many different types of flyball governors exist, however they all operate under the same basic principle: two weighted flyballs rotate around a central shaft relative to the speed of rotation of the object they are controlling, the height that the weights rotate around the shaft at changes based on this rotational speed, and this in turn controls how much working fluid is admitted (the higher the balls, the less fluid is admitted) [2]. The main types of flyball governors are: the Watt governor; the Porter governor; the Proell governor; and the Hartnell governor.

2.1.1 The Watt Governor

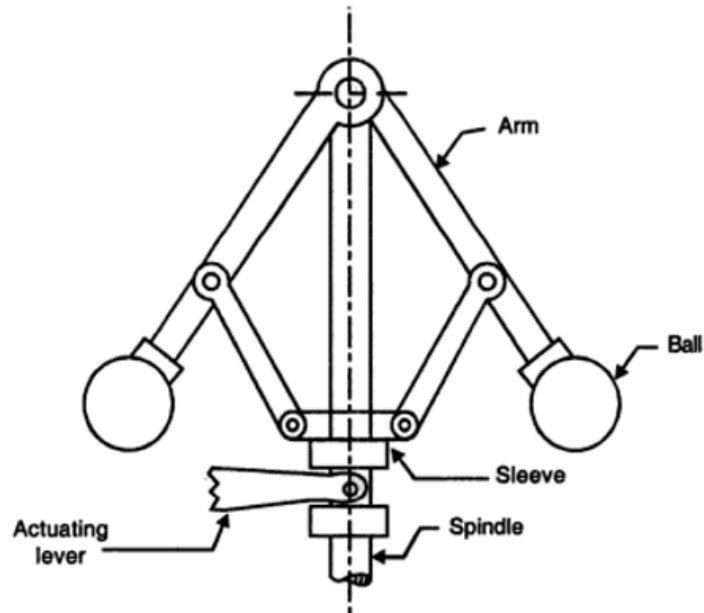


Figure 2.1: Watt Governor [2]

The Watt governor is the most well-known type of flyball governor, being invented by James Watt in 1788 to be used in steam engines. As seen in Figure 2.1 above, the Watt governor is the simplest type of governor, consisting of two arms that are connected together at one end at the top of the central shaft, and have a flyball attached to the other end. Two links connect the arms to a sleeve that is allowed to move up and down the shaft based on the speed of rotation of the balls, and controls the amount of working fluid that is admitted to the system [2]. Note that the links may also be attached to the flyballs themselves instead of the arms. The Watt governor will be the focus of this research.

2.1.2 The Porter Governor

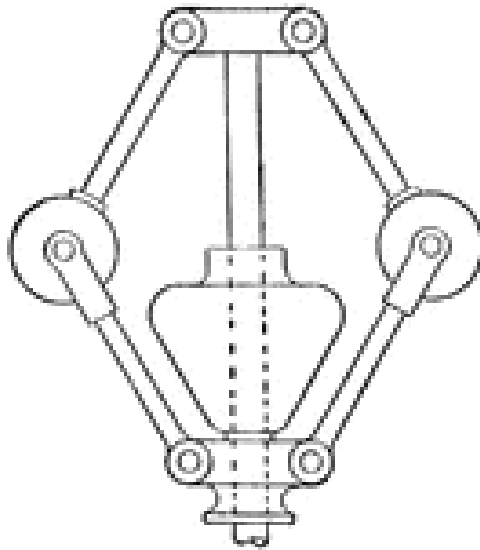


Figure 2.2: Porter Governor [3]

The Porter governor, as seen in Figure 2.2 above, is very similar to a Watt governor except that it has the addition of a large weight connected to the sliding sleeve. This weight provides a constant downwards load to the system which makes the governor able to operate better at higher rotational speeds [2].

2.1.3 The Proell Governor

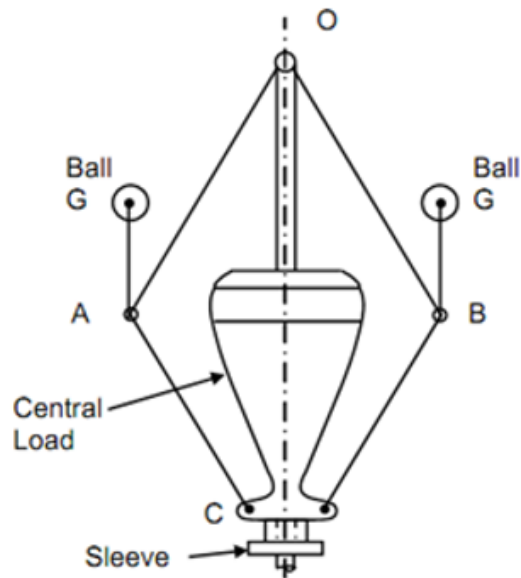


Figure 2.3: Proell Governor [4]

The Proell governor shown in Figure 2.3 above is also very similar to the Watt governor, except that it has a heavy weight attached to the central sleeve similarly to the Porter governor, and that the flyball are attached to extensions above the point where the arms and links join. The governor is designed such that the extensions are vertical when operating at the normal rotational speeds [2].

2.1.4 The Hartnell Governor

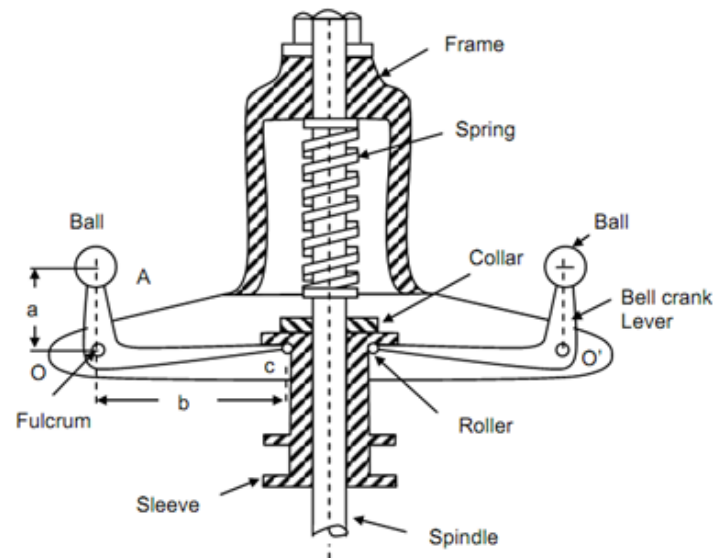


Figure 2.4: Hartnell Governor [5]

The Hartnell governor, as seen in Figure 2.4 above, is different to the Watt governor as it also possesses a spring mechanism, which acts in a similar manner to the load in the Porter and Proell governors. Instead of changing the height that the balls rotate at, the centrifugal force forces the balls to rotate further away from the central shaft, which causes the bell crank lever that the balls are attached to rotate around the pivot point and force the sleeve up, against the force of the spring. The sleeve again controls the amount of working fluid is admitted (the higher the sleeve is, the less fluid is admitted) [2].

2.2 Stability

Stability is a property of the trajectories of a dynamic system; if a trajectory is stable, then a minor disturbance will result in only a minor change in the trajectory. The result could be either that a new steady trajectory, close to the original one, will be reached, or that the system will approach the old trajectory over time. A system may be called stable if, for a specific operating point, the resultant trajectories are stable [6].

There are many different ways to determine stability in the form of stability criterion, and the two that will be used in this paper are Routh's stability criterion and Maxwell's stability

criterion. Additionally, the model and stability criterion found in this paper will be compared to those found by Denny [7] (who employed a similar engine-governor model) to ensure validity.

2.2.1 Routh Stability

Routh's stability criterion as they are used in this paper are related to the implementation of the method of Routh reduction in deriving the reduced equations of motion in conjunction with the Euler-Lagrange formalism. Routh reduction involves exploiting symmetries within a system, that is, expressing coordinates within a dynamic for which momentum is conserved (called cyclic coordinates) in terms of this constant value [8]. Doing this results in a Routhian that is dependent on less variables than the associated Lagrangian (as the cyclic coordinates have been eliminated), whilst also having a different potential term, that is called the amended potential term. A more formal and mathematical description of this method, as well as its implementation, is provided in Chapters 3 and 4. Finally, Routh's stability criterion states that stable trajectories are those for which the second derivative of the amended potential is positive definite [8].

2.2.2 Maxwell Stability

Maxwell's stability criterion were developed by Maxwell as part of his analysis of flyball governors in his famous paper *On Governors*, published in 1867 [9]. Maxwell had identified that the motion of an engine-governor system that has been disturbed could take on a number of different forms, those being that: the magnitude of the disturbance will continuously grow; the magnitude of the disturbance will decrease; the motion will be oscillatory in nature that grows in value; the motion will be oscillatory in nature that decreases over time; or any combination of these forms. Maxwell then went on to conclude that for a governor to be stable, only the second and fourth forms of motion could be present. The paper continues to examine the stability of engine-governor systems and derives a mathematical dynamic model for the system. Maxwell uses this model to create a set of constraints for the system parameters that will make the roots negative, and thus the trajectories stable [9]. Chapter 4 provides a more in-depth mathematical derivation for Maxwell's stability criterion as they relate to this model.

2.3 Digital Feedback Control Mechanisms

2.3.1 Feedback

The term 'feedback' refers to the act of using some, or all, of the outputs of a system as inputs in order to affect the next set of outputs, that is, the outputs are 'fed back' into the system. The concept of feedback and use of feedback systems, whilst existing beforehand, became popular in the 20th Century and since then has been used in a multitude of different academic disciplines. Two types of feedback exist: positive, which is when the feedback loop amplifies changes in the input; and negative, where the feedback loop resists changes in the input. Feedback serves as a major focus in the area of control theory, where the type of feedback used is predominately negative. In one aspect of control theory, a device called a controller is inserted into the feedback loop in order to control the outputs of the system (called the plant), as well as how the system reacts to changes in the inputs [6] [10]. Such a device is known as a digital feedback controller.

2.3.2 PID Controllers

One very common type of digital feedback controller is the PID (Proportional, Integral, Derivative) Controller. The main aim of the PID controller is to minimise the error between the measured value of a set of input signals and a pre-defined desired value. The equation for a PID controller is given in [11] as ($e(t)$ is the error at time t):

$$C_{PID} = k_p e(t) + k_i \int_0^t e(\tau) d\tau + k_d \frac{d}{dt} e(t) \quad (2.1)$$

The three components of a PID controller all perform different tasks, and not all of them need be used in every PID controller, for example, to control a specific system a PD controller may be all that is needed.

The P element is the proportional element. It is dependent upon the current error in the system and is used to control the responsiveness of the system to changes in the input. The I element is the integral element. It is dependent upon the accumulated past error in the system and is used to eliminate the steady-state error introduced by a pure proportional controller. The D element is the derivative element. It is dependent upon the future error of the system and is used to improve the settling time and stability of the system [11].

A Dynamic Model for a Watt Engine-Governor System

In this chapter, a dynamic model for both the Watt governor and the steam engine is developed using the method of Routh reduction. A joint model is then produced via two methods: combining the reduced models for the governor and engine; and creating a model for the combined system independently before performing Routh reduction; and it is shown that these two methods produce the same result. Finally, a brief introduction to Watt governor design is provided that focusses on generating the desired velocity profile. The models developed in this chapter will be used in the next chapter to perform a stability analysis of the governor and the joint system.

3.1 Dynamic Model for the Watt Governor

In order to do any analysis of the flyball governor system, the most important step that needs to be completed is to determine the equations of motion. One way to do this is to apply the Euler-Lagrange formalism as in [12]. This is done by first choosing a set of independent generalised coordinates that fully describe the state of the system, as well as a set of admissible variations and given that the system is holonomic (the number of coordinates matches the number of variations), the rest of the formalism may then be applied. The generalised forces for each coordinate are computed by calculating the variational non-conservative work term and setting it equal to the sum of the generalised force terms. The Lagrangian \mathcal{L} for the system is then calculated by computing the kinetic co-energy (T^*) and potential energy (V)

terms, and setting $\mathcal{L} = T^* - V$. Finally the equations of motion are given by:

$$\frac{d}{dt} \left(\frac{\partial \mathcal{L}}{\partial \dot{x}_i} \right) - \frac{\partial \mathcal{L}}{\partial x_i} = \Xi_{x_i}, \quad (3.1)$$

where x_i represents a coordinate (so there will be as many equations of motion as there are coordinates), and Ξ_{x_i} is the generalised force for coordinate x_i .

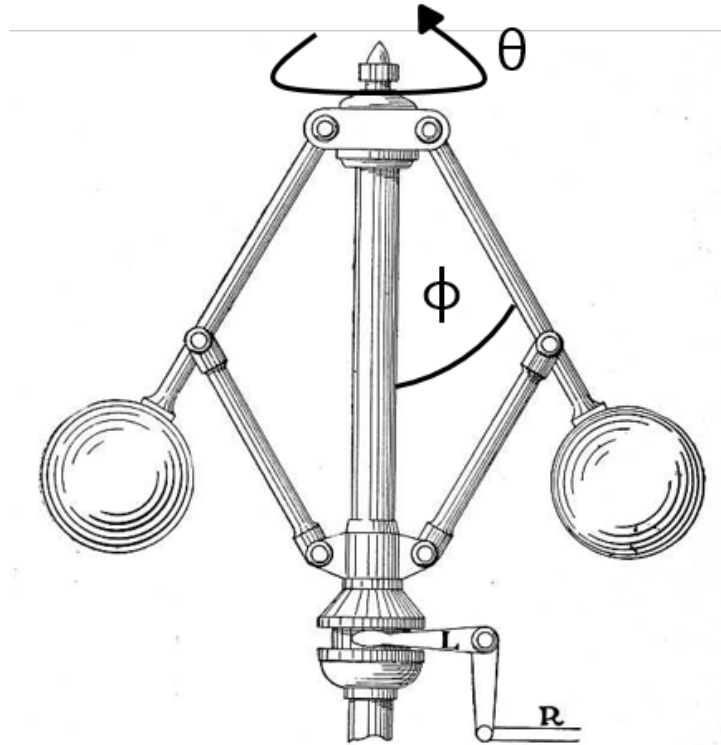


FIG. 15—A FLY-BALL GOVERNOR

Figure 3.1: Image Showing Choice of Coordinates for Euler-Lagrange Formalism

For this derivation, the coordinates chosen were the angle of the flyball connecting rod around the central shaft measured positive counter-clockwise (denoted θ), and the angle that the connecting rod makes with the vertical edge of the central shaft measured positive from the vertical (denoted ϕ). The choice of coordinates is illustrated in Figure 3.1 above. The admissible variations are then $\delta\theta$ and $\delta\phi$, and as the number of admissible variations is equal to the number of coordinates the system is holonomic, and the rest of the formalism may be applied.

The following table (Table 3.1) and diagram (Figure 3.2) detail some of the nomenclature used

in this derivation.

Table 3.1: Nomenclature

Parameter	Description
c_1	Friction Coefficient (of Sleeve and Central Shaft)
c_2	Torsional Friction Coefficient (of Rotation around Central Shaft)
c_3	Engine Rotation Speed (ω) to Governor Rotation Speed ($\dot{\theta}$) Conversion Factor ($\dot{\theta} = c_3\omega$)

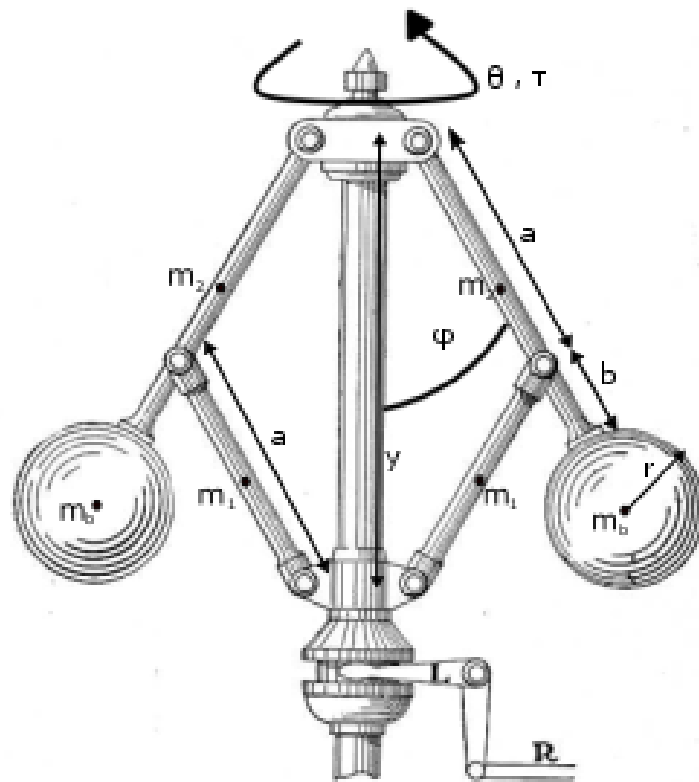


FIG. 15—A FLY-BALL GOVERNOR

Figure 3.2: Image Showing Parameters used during derivation of equation of motion

3.1.1 Generalised Forces

To simplify the calculations, a (the distance between the top of the central shaft and the point where the flyball arm meets the connecting arm) was assumed to be equal to l (the length of the connecting arm), however this is not the case in general.

The variational non-conservative work relates to the generalised forces via

$$\delta W^{nc} = \Xi_{\theta} + \Xi_{\phi}. \quad (3.2)$$

The following equation is then obtained

$$\delta W^{nc} = \tau \delta \theta - c_1 \dot{y} \delta y - c_2 \dot{\theta} \delta \theta$$

where

$$y = 2a \cos \phi$$

$$\dot{y} = -2a \sin \phi \dot{\phi}$$

$$\delta y = -2a \sin \phi \delta \phi$$

and hence

$$\therefore \delta W^{nc} = \tau \delta \theta - 4a^2 c_1 \sin^2 \phi \dot{\phi} \delta \phi - c_2 \dot{\theta} \delta \theta. \quad (3.3)$$

Equating equation (3.3) and equation (3.2) and using independence gives the following two results:

$$\Xi_{\theta} = \tau - c_2 \dot{\theta} \quad (3.4)$$

and

$$\Xi_{\phi} = -4a^2 c_1 \sin^2 \phi \dot{\phi} \quad (3.5)$$

3.1.2 Lagrangian

Inertia of the Ball

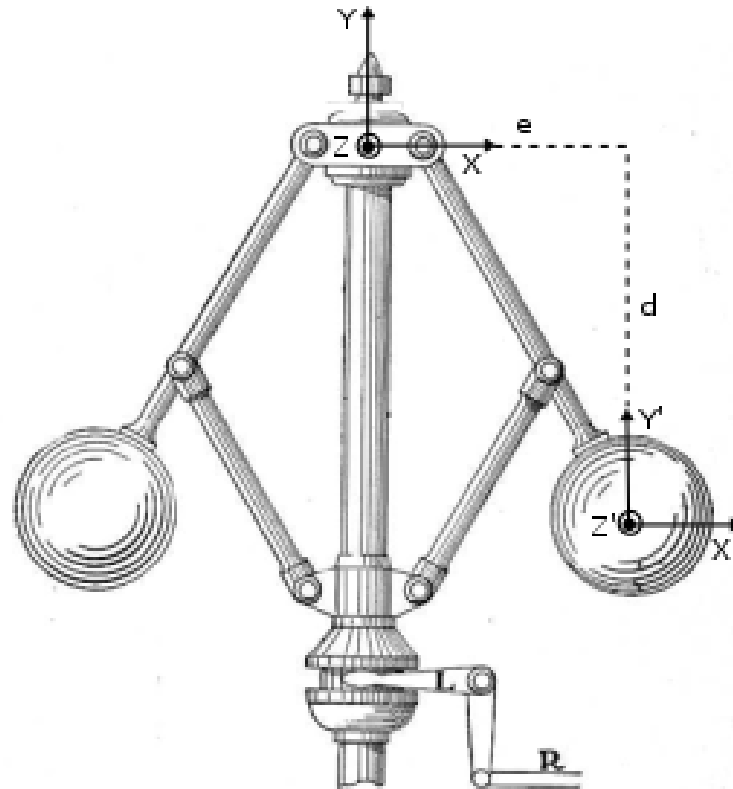


FIG. 15—A FLY-BALL GOVERNOR

Figure 3.3: Image Showing Choice of Frames for Parallel Axis Theorem

To find the inertia of the ball as it rotates around the vertical shaft the parallel axis theorem is used (to account for the ball having both rotational and translational motion). The inertial point of reference chosen was the top of the vertical shaft, and the vector that connects this point to the centre of the right ball is:

$$\begin{pmatrix} d \\ e \\ f \end{pmatrix} = \begin{pmatrix} (a + b + r) \sin \phi \\ -(a + b + r) \cos \phi \\ 0 \end{pmatrix}. \quad (3.6)$$

The vector that connects the top of the shaft to the centre of the left ball is:

$$\begin{pmatrix} d \\ e \\ f \end{pmatrix} = \begin{pmatrix} -(a+b+r) \sin \phi \\ -(a+b+r) \cos \phi \\ 0 \end{pmatrix}. \quad (3.7)$$

The parallel axis theorem gives an expression for the inertia $[I]_B$ of the ball around the central shaft:

$$[I]_B = [I]_C + m_b \begin{bmatrix} e^2 + f^2 & -de & -df \\ -de & f^2 + d^2 & -ef \\ -df & -ef & d^2 + e^2 \end{bmatrix}, \quad (3.8)$$

where m_b is the mass of the ball, d , e and f are as shown in equation (3.6) (and equation (3.7)) and $[I]_C$ represents the inertia of the ball rotating around its centre of mass and is given by:

$$[I]_C = \begin{bmatrix} \frac{2m_b r^2}{5} & 0 & 0 \\ 0 & \frac{2m_b r^2}{5} & 0 \\ 0 & 0 & \frac{2m_b r^2}{5} \end{bmatrix}. \quad (3.9)$$

The inertia of the right ball is:

$$[I]_{B_r} = \begin{bmatrix} \frac{2m_b r^2}{5} + m_b(a+b+r)^2 \cos^2 \phi & m_b(a+b+r)^2 \sin \phi \cos \phi & 0 \\ m_b(a+b+r)^2 \sin \phi \cos \phi & \frac{2m_b r^2}{5} + (a+b+r)^2 \sin^2 \phi & 0 \\ 0 & 0 & \frac{2m_b r^2}{5} + m_b(a+b+r)^2 \end{bmatrix} \quad (3.10)$$

and similarly for the left ball.

The velocity vector of the ball on the right is:

$$\omega_r = \begin{pmatrix} 0 \\ \dot{\theta} \\ \dot{\phi} \end{pmatrix} \quad (3.11)$$

And the velocity vector for the ball on the left is:

$$\omega_l = \begin{pmatrix} 0 \\ \dot{\theta} \\ -\dot{\phi} \end{pmatrix} \quad (3.12)$$

Kinetic co-energy is given by:

$$T^* = \frac{1}{2} \omega^T [I]_B \omega \quad (3.13)$$

Therefore the kinetic co-energy of the right ball is:

$$T_{b,r}^* = \frac{m_b r^2}{5} \dot{\theta}^2 + \frac{1}{2} m_b (a + b + r)^2 \sin^2 \phi \dot{\theta}^2 + \frac{m_b r^2}{5} \dot{\phi}^2 + \frac{1}{2} m_b (a + b + r)^2 \dot{\phi}^2 \quad (3.14)$$

Similarly, the kinetic co-energy for the left ball is:

$$T_{b,l}^* = \frac{m_b r^2}{5} \dot{\theta}^2 + \frac{1}{2} m_b (a + b + r)^2 \sin^2 \phi \dot{\theta}^2 + \frac{m_b r^2}{5} \dot{\phi}^2 + \frac{1}{2} m_b (a + b + r)^2 \dot{\phi}^2 \quad (3.15)$$

And so, the total kinetic co-energy of the two flyballs is:

$$T_b^* = \frac{2m_b r^2}{5} \dot{\theta}^2 + m_b (a + b + r)^2 \sin^2 \phi \dot{\theta}^2 + \frac{2m_b r^2}{5} \dot{\phi}^2 + m_b (a + b + r)^2 \dot{\phi}^2 \quad (3.16)$$

Inertia of the Rods

Similar to the calculation of the inertia of the balls, the inertia of the rods as they rotate around the central shaft may be calculated using the same reference frames. The inertia tensor matrix of a rod rotating around a point at one of its ends is given by:

$$[I]_B = \begin{bmatrix} \frac{ml^2}{3} \cos^2 \phi & \frac{ml^2}{6} \sin 2\phi & 0 \\ \frac{ml^2}{6} \sin 2\phi & \frac{ml^2}{3} \sin^2 \phi & 0 \\ 0 & 0 & \frac{ml^2}{3} \end{bmatrix} \quad (3.17)$$

where l is the length of the rod, and m is the mass of the rod.

The velocity vector(s) from equation (3.11) (and (equation 3.12)) remain unchanged for

the rods.

Substituting the values for the flyball arms into equation (3.17) gives the inertia tensor matrix for these pair of rods. The result for the right rod is:

$$\left[I \right]_{B_r} = \begin{bmatrix} \frac{m_2}{3}(a+b)^2 \cos^2 \phi & \frac{m_2}{6}(a+b)^2 \sin 2\phi & 0 \\ \frac{m_2}{6}(a+b)^2 \sin 2\phi & \frac{m_2}{3}(a+b)^2 \sin^2 \phi & 0 \\ 0 & 0 & \frac{m_2}{3}(a+b)^2 \end{bmatrix} \quad (3.18)$$

And the result for the left rod is:

$$\left[I \right]_{B_l} = \begin{bmatrix} \frac{m_2}{3}(a+b)^2 \cos^2 \phi & -\frac{m_2}{6}(a+b)^2 \sin 2\phi & 0 \\ -\frac{m_2}{6}(a+b)^2 \sin 2\phi & \frac{m_2}{3}(a+b)^2 \sin^2 \phi & 0 \\ 0 & 0 & \frac{m_2}{3}(a+b)^2 \end{bmatrix} \quad (3.19)$$

Therefore the total kinetic co-energy for this pair of rods is equal to:

$$T_{rod2}^* = \frac{m_2}{3}(a+b)^2 \sin^2 \phi \dot{\theta}^2 + \frac{m_2}{3}(a+b)^2 \dot{\phi}^2 \quad (3.20)$$

For the other pair of rods (the connecting arms) the inertial point of reference chosen was the sleeve. The inertia tensor matrix for the right rod is:

$$\left[I \right]_{B_r} = \begin{bmatrix} \frac{m_1}{3}a^2 \cos^2 \phi & \frac{m_1}{6}a^2 \sin 2\phi & 0 \\ \frac{m_1}{6}a^2 \sin 2\phi & \frac{m_1}{3}a^2 \sin^2 \phi & 0 \\ 0 & 0 & \frac{m_1}{3}a^2 \end{bmatrix} \quad (3.21)$$

And the inertia tensor matrix for the left rod is:

$$\left[I \right]_{B_l} = \begin{bmatrix} \frac{m_1}{3}a^2 \cos^2 \phi & -\frac{m_1}{6}a^2 \sin 2\phi & 0 \\ -\frac{m_1}{6}a^2 \sin 2\phi & \frac{m_1}{3}a^2 \sin^2 \phi & 0 \\ 0 & 0 & \frac{m_1}{3}a^2 \end{bmatrix} \quad (3.22)$$

Thus the total kinetic co-energy for this pair of rods is given by:

$$T_{rod1}^* = \frac{m_1}{3}a^2 \sin^2 \phi \dot{\theta}^2 + \frac{m_1}{3}a^2 \dot{\phi}^2 \quad (3.23)$$

Summing the three terms together gives the total kinetic co-energy of the system:

$$\begin{aligned}
 T^* &= T_b^* + T_{rod1}^* + T_{rod2}^* \\
 &= \frac{2m_b r^2}{5} \dot{\theta}^2 + m_b (a + b + r)^2 \sin^2 \phi \dot{\theta}^2 + \frac{2m_b r^2}{5} \dot{\phi}^2 + m_b (a + b + r)^2 \dot{\phi}^2 \\
 &\quad + \frac{m_1}{3} a^2 \sin^2 \phi \dot{\theta}^2 + \frac{m_1}{3} a^2 \dot{\phi}^2 + \frac{m_2}{3} (a + b)^2 \sin^2 \phi \dot{\theta}^2 + \frac{m_2}{3} (a + b)^2 \dot{\phi}^2
 \end{aligned} \tag{3.24}$$

Potential Term

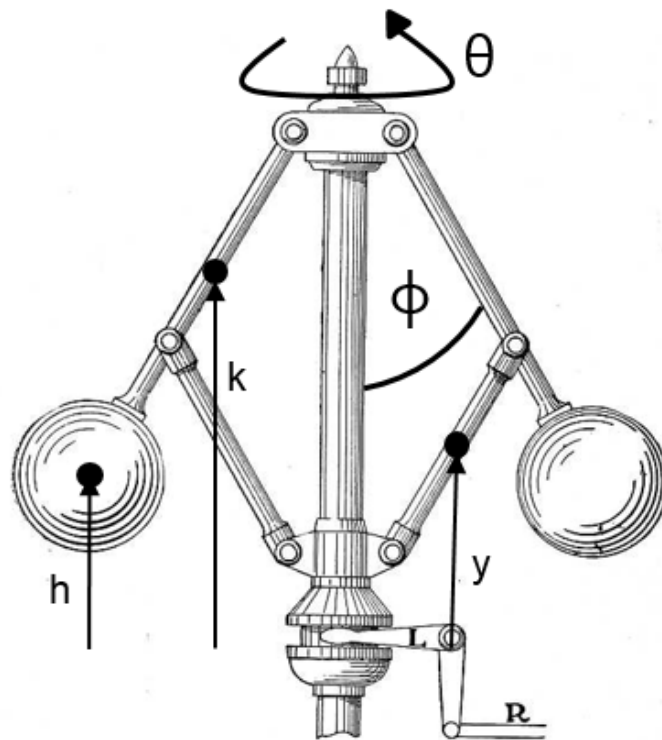


FIG. 15—A FLY-BALL GOVERNOR

Figure 3.4: Image Showing Choice of Parameters Used for Calculating Potential Term

For this system, the zero potential was chosen as the state of the system when ϕ was equal to 0. Using the above diagram (Figure 3.4), the potential term of the system may then be written as:

$$V = 2m_bgh + 2m_1gy + 2m_2gk$$

$$h = (a + b + r) - (a + b + r) \cos \phi$$

$$y = \frac{3a}{2} - \frac{3a}{2} \cos \phi$$

$$k = \frac{a + b}{2} - \frac{a + b}{2} \cos \phi$$

$$\therefore V = 2m_bg((a + b + r) - (a + b + r) \cos \phi) + 2m_1g\left(\frac{3a}{2} - \frac{3a}{2} \cos \phi\right) + 2m_2g\left(\frac{a + b}{2} - \frac{a + b}{2} \cos \phi\right) \quad (3.25)$$

Lagrangian

Substituting equations (3.24) and (3.25) into the equation for the Lagrangian gives the following result:

$$\begin{aligned} \mathcal{L} = & \frac{2m_b r^2}{5} \dot{\theta}^2 + m_b(a + b + r)^2 \sin^2 \phi \dot{\theta}^2 + \frac{2m_b r^2}{5} \dot{\phi}^2 + m_b(a + b + r)^2 \dot{\phi}^2 \\ & + \frac{m_1}{3} a^2 \sin^2 \phi \dot{\theta}^2 + \frac{m_1}{3} a^2 \dot{\phi}^2 + \frac{m_2}{3} (a + b)^2 \sin^2 \phi \dot{\theta}^2 + \frac{m_2}{3} (a + b)^2 \dot{\phi}^2 \\ & - 2m_bg(a + b + r) + 2m_bg(a + b + r) \cos \phi - 3am_1g + 3am_1g \cos \phi \\ & - m_2g(a + b) + m_2g(a + b) \cos \phi \end{aligned} \quad (3.26)$$

Defining the following parameters to simplify further equations:

$$\begin{aligned}
 M_r &= \frac{4m_b r^2}{5} \\
 M_b &= 2m_b(a + b + r)^2 \\
 M_1 &= \frac{2}{3}m_1 a^2 \\
 M_2 &= \frac{2}{3}m_2(a + b)^2 \\
 C_m &= M_b + M_1 + M_2 \\
 M &= M_r + M_b + M_1 + M_2 \\
 C_g &= 2m_b g(a + b + r) + 3am_1 g + m_2 g(a + b)
 \end{aligned}$$

The Lagrangian may then be rewritten as

$$\mathcal{L} = \frac{M_r}{2}\dot{\theta}^2 + \frac{C_m}{2}\sin^2\phi\dot{\theta}^2 + \frac{M}{2}\dot{\phi}^2 + C_g \cos\phi - C_g \quad (3.27)$$

3.1.3 Routh Reduction

Reduced Lagrangian

Upon examination of the Lagrangian developed above in equation (3.27) it is obvious that $\dot{\theta}$ appears, while θ does not. Thus θ is a cyclic coordinate in this equation and the method of Routh reduction [8] may be applied.

The momentum associated with the cyclic coordinate θ is:

$$\begin{aligned}
 p &= \frac{\partial \mathcal{L}}{\partial \dot{\theta}} \\
 &= M_r \dot{\theta} + C_m \sin^2\phi \dot{\theta} =: \mu
 \end{aligned} \quad (3.28)$$

Assuming p to be constant ($=\mu$), this generates an expression for the variable $\dot{\theta}$:

$$\dot{\theta} = (M_r + C_m \sin^2\phi)^{-1} \cdot \mu = \frac{\mu}{C_p(\phi)} \quad (3.29)$$

where

$$C_p(\phi) = M_r + C_m \sin^2 \phi. \quad (3.30)$$

Note that expanded forms of this value and its derivatives are provided in the Appendices. The reduced form of the Lagrangian is then given by substituting this result into:

$$R = \mathcal{L} - \mu\dot{\theta} \quad (3.31)$$

$$\begin{aligned} \therefore R &= \frac{1}{2}(M_r + C_m \sin^2 \phi) \cdot \frac{\mu^2}{C_p^2(\phi)} + \frac{M}{2}\dot{\phi}^2 - \frac{\mu^2}{C_p(\phi)} - V \\ &= \frac{1}{2}C_p(\phi) \cdot \frac{\mu^2}{C_p^2(\phi)} + \frac{M}{2}\dot{\phi}^2 - \frac{\mu^2}{C_p(\phi)} - V \\ &= \frac{M}{2}\dot{\phi}^2 - \frac{\mu^2}{2C_p(\phi)} - V \\ &= \frac{M}{2}\dot{\phi}^2 - V_\mu(\phi) \end{aligned} \quad (3.32)$$

where $V_\mu(\phi)$ is the amended potential and is given by:

$$V_\mu(\phi) = \frac{\mu^2}{2C_p(\phi)} + V \quad (3.33)$$

Here, V is the original potential as defined in equation (3.25), and is equivalent to $C_g - C_g \cos \phi$.

Note that expanded forms of this amended potential and its derivatives are provided in the Appendices.

Reduced Euler-Lagrange Equations

The reduced Euler-Lagrange Equations can now be found by applying the rest of the Euler-Lagrange formalism to the Routhian.

$$\frac{\partial R}{\partial \phi} = M\dot{\phi} \quad (3.34)$$

$$\frac{d}{dt} \left(\frac{\partial R}{\partial \dot{\phi}} \right) = M\ddot{\phi} \quad (3.35)$$

$$\frac{\partial R}{\partial \phi} = -V'_\mu(\phi) = \frac{\mu^2 C'_p(\phi)}{2C_p^2(\phi)} - 2m_b g(a+b+r) \sin \phi - 3am_1 g \sin \phi - m_2(a+b)g \sin \phi \quad (3.36)$$

Therefore, by substituting the above equations into equation (3.1), the equation of motion for the reduced system may be attained:

$$M\ddot{\phi} + V'_\mu(\phi) = -4a^2 c_1 \sin^2 \phi \dot{\phi}. \quad (3.37)$$

It can be seen that this equation has the form of a rotating harmonic oscillator with friction, which makes intuitive sense given the nature of the system.

3.2 Dynamic Model for the Joint System

3.2.1 Dynamic Model for the Engine

In order to examine the stability of the combined engine-governor system, a dynamic model that represents the joint system must be developed. To do this, a very simple engine model is provided:

$$I\dot{\omega} = Kh(\phi) - \tau, \quad (3.38)$$

where ω is the engine rotational speed, I is the engine moment of inertia, K is a constant relating sleeve height to engine torque, and τ is the engine load torque.

3.2.2 Combining the Models

Therefore, the equations of motion of the joint system are:

$$\ddot{\phi} = \frac{(c_3\omega)^2 M_b \sin \phi \cos \phi}{M_r + M_b} - \frac{M_g \sin \phi}{M_r + M_b} - \frac{f(\phi, \dot{\phi})}{M_r + M_b} \quad (3.39)$$

$$\dot{\omega} = \frac{K}{I} (h(\phi) - h(\hat{\phi})) \quad (3.40)$$

where $c_3\omega = \dot{\theta}$, $M_g = 2m_b g(a + b + r)$, $f(\phi, \dot{\phi})$ is the frictional term caused by the movement of the sleeve against the shaft, $\tau = Kh(\hat{\phi})$, and the masses m_1, m_2 have been assumed to be negligible.

Comparing this to the equations of motions developed by Denny [7] shows that the two are very similar, the main differences arising from: the use of different frictional terms; this model assuming the distance between where the arms of the flyball connect at the top of the shaft is negligible; and a different mass term arising from the more complicated model in this paper. The fact that the two sets of equations have the same essential components helps to ensure the validity of this derived model.

3.2.3 Alternative Joint Model Derivation

Engine Lagrangian

Alternatively, the equations of motion for the joint engine-governor system can be derived from the combined Lagrangian.

The engine model used is that of a simple flywheel rotating around a single shaft. The input torque to the engine is provided at a rate relative to the governor angle ϕ , and there is an external load torque that resists the engine's rotation. The speed of rotation of the governor is set by the speed of rotation of the engine (i.e. $\dot{\theta}$ is dependent on ω).

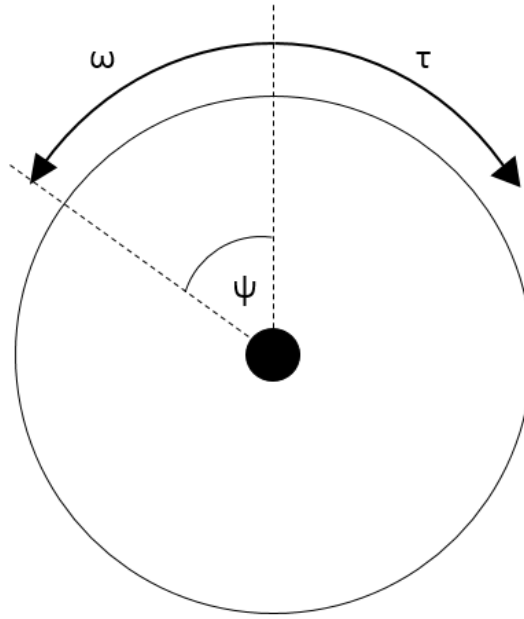


Figure 3.5: Engine Diagram

It is clear that the only energy term that is added by including the engine, is the rotational energy term. Thus the energy terms for the combined system are:

$$T_{comb}^* = \frac{1}{2}I\omega^2 + T^* \quad (3.41)$$

$$V_{comb} = V \quad (3.42)$$

where T^* and V are the energy terms for the governor, I is the moment of inertia of the engine, and $\omega = \dot{\psi}$ is the rotational speed of the engine.

There is also an additional generalised force:

$$\Xi_{\psi} = Kh(\phi) - \tau \quad (3.43)$$

where $Kh(\phi)$ is the input torque, and τ is the engine load.

Thus the Lagrangian for the combined system is:

$$\mathcal{L}_{comb} = \frac{1}{2}I\omega^2 + \mathcal{L} \quad (3.44)$$

where \mathcal{L} is the Lagrangian for the governor.

Engine Routhian

It is obvious that the combined Lagrangian still has the cyclic coordinate θ , and so the method of Routh reduction may again be applied. Also, as the only additional term in the combined Lagrangian does not depend on $\dot{\theta}$, the conserved momentum term μ is unchanged. Therefore, the reduced form of the Lagrangian is

$$\begin{aligned} R_{comb} &= \mathcal{L}_{comb} - \mu\dot{\theta} \\ &= \frac{1}{2}I\omega^2 + \mathcal{L} - \mu\dot{\theta} \\ &= \frac{1}{2}I\omega^2 + R \end{aligned} \quad (3.45)$$

where R is the Routhian for the governor.

So, the reduced Euler-Lagrange equations are

$$\begin{aligned} M\ddot{\phi} + V'_\mu(\phi) &= -4a^2c_1 \sin^2 \phi \dot{\phi} \\ I\dot{\omega} &= Kh(\phi) - \tau \end{aligned} \quad (3.46)$$

Substituting in the value for V'_μ and using $C_g = 2m_b g(a + b + r) + 3am_1 g + m_2 g(a + b)$ and $f(\phi, \dot{\phi}) = 4a^2c_1 \sin^2 \phi \dot{\phi}$ gives:

$$\begin{aligned} M\ddot{\phi} + \frac{\mu^2 C'_p(\phi)}{2C_p^2(\phi)} - C_g \sin \phi &= -f(\phi, \dot{\phi}) \\ I\dot{\omega} &= Kh(\phi) - \tau \end{aligned} \quad (3.47)$$

Recall that $c_3\omega = \dot{\theta} = \frac{\mu}{C_p(\phi)}$, thus the equations may be written as:

$$\begin{aligned} M\ddot{\phi} + (c_3\omega)^2 C_m \sin \phi \cos \phi - C_g \sin \phi &= -f(\phi, \dot{\phi}) \\ I\dot{\omega} &= Kh(\phi) - \tau \end{aligned} \quad (3.48)$$

Finally, by rearranging the equations and using the substitutions $m_1 = m_2 = 0$, $M_g = 2m_b g(a + b + r)$ and $\tau = Kh(\hat{\phi})$, the following is obtained:

$$\ddot{\phi} = \frac{(c_3\omega)^2 M_b \sin \phi \cos \phi}{M_r + M_b} - \frac{M_g \sin \phi}{M_r + M_b} - \frac{f(\phi, \dot{\phi})}{M_r + M_b}$$

$$\dot{\omega} = \frac{K}{I}(h(\phi) - h(\hat{\phi}))$$

which is the same result as was obtained before in equation (3.39).

This model will be used in the next chapter to perform a stability analysis of both the governor and the joint system.

3.3 Watt Governor Design

An examination of the steady-state operation of the governor using the dynamic model developed above may be performed to investigate some aspects fo Watt governor design. The two aspects focussed on in this paper were to show that the negligible rod mass assumption is valid, and to determine basic realtionships between the individual governor parameters and resultant velocity profile.

3.3.1 Validation of Negligible Rod Mass Assumption

In Figure 3.6 below, the blue line represents the case where rod mass is equal to zero, the magenta line represents the case where the ratio of rod mass to ball mass is 1:20, the green line represents the case where this ratio is 1:10, and the red line is the case where the ratio is 1:40.

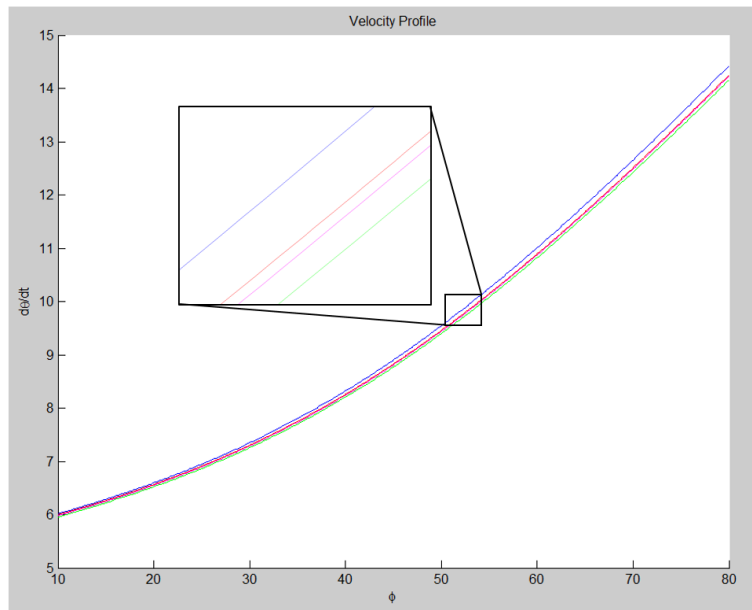


Figure 3.6: Velocity Profile - Changing Rod Mass

From this plot, it is immediately clear that the addition of non-zero rod mass to the system has minimal impact on the resultant velocity. It can also be seen that the velocity profile shifts downward as the rod mass increases, and that the difference is greater as the critical angle increases. This means that the assumption is more valid for lower values of $\hat{\phi}$. Based on these results, it can be concluded that as long as the flyball mass is at least ten times greater than the rod mass, then assuming the rod mass is negligible will have minimal impact on calculations and is a valid assumption.

3.3.2 Effect of Governor Parameters

In Figure 3.7 below, the blue line represents the default case, the red line represents the case where the governor arm length has been doubled, the green line represents the case where the governor arm length has been halved.

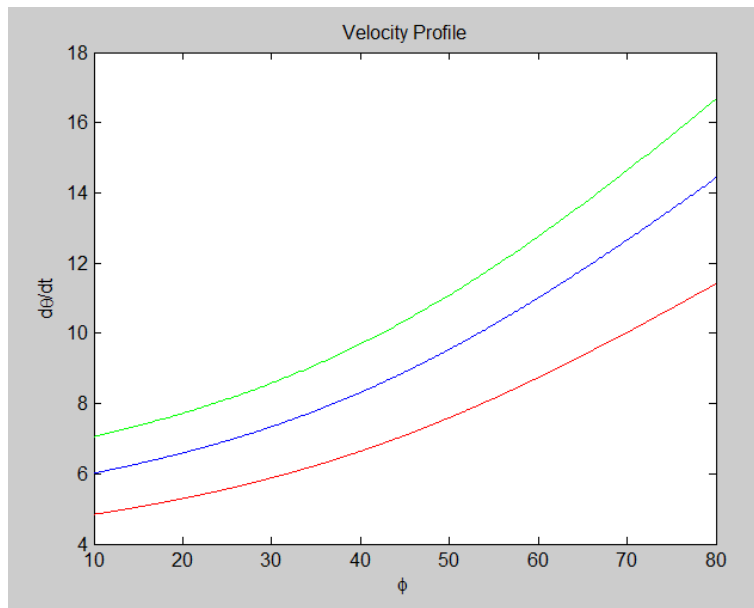


Figure 3.7: Velocity Profile - Changing Governor Arm Length

Note that the plots for varying governor arm extension length and flyball radius are similar and are provided in the Appendices.

From this plot, it is obvious that the velocity profile for the governor is inversely related to the governor arm length, and the other plots showed that this held true for governor arm extension and flyball radius as well. It is also observed that the profile shift caused by halving a parameter is generally less than the shift caused by doubling a parameter, showing that the relationship is not proportional. Varying the governor arm length was seen to cause the largest shift in the velocity profile, whilst varying flyball radius had the least impact, which makes intuitive sense given the nature of the system.

Velocity Dependence

The graph below (Figure 3.8) shows how specific points change as each of the governor arm length is varied. The points examined were the 'minimum' point (the velocity at $\phi = 10^\circ$, represented by an orange line), the 'operating' point (the velocity at $\phi = 45^\circ$, represented by a gray line) and the 'maximum' point (the velocity at $\phi = 80^\circ$, represented by a blue line).

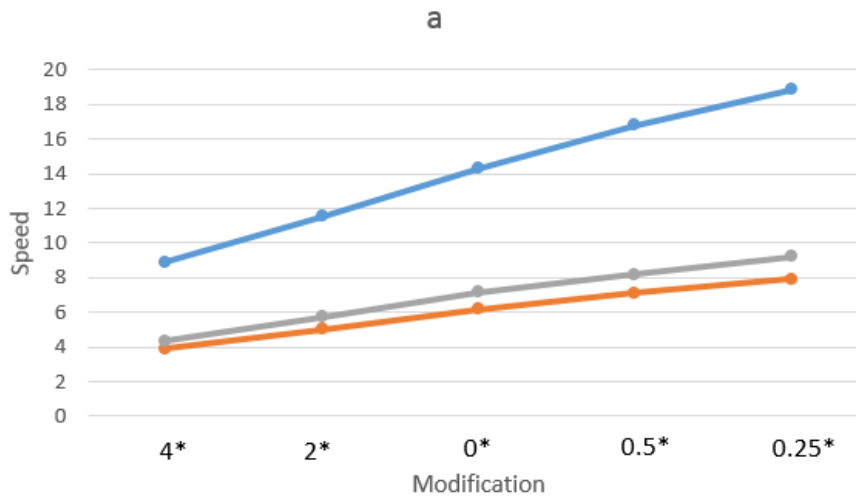


Figure 3.8: Velocity Graph - Changing Governor Arm Length

Note that the graphs for the other variables are similar and are provided in the Appendices. This graph shows that the length of the governor arm decreases, the speed at which the engine rotates increases, and that this increase is larger for higher values of $\hat{\phi}$. It was observed that varying the governor arm length had the largest individual impact on the velocity profile, whilst varying flyball radius had the least. Additionally it was found that the individual changes in each of the individual parameters (for the individual points) all appear to linearly affect the speed at which the governor rotates.

Another simulation was performed in which both governor arm length and governor arm extension were varied simultaneously, and it was found that the velocity function was not a linear combination of these variables. The results of this simulation are provided in the Appendices.

Stability Analysis

In this chapter, a stability analysis for the governor is performed using the Routh stability criterion, for which the governor is found to be stable for all practical combinations of variables. A stability analysis is then performed on the joint-model using the Maxwell stability criteria, for which a set of two conditions for stability are found. Finally, an investigation of the transient response of the system to a disturbance in engine load was conducted, and the system was found to be under-damped for all possible cases. The model used to test the transient response is used as the basis for developing a similar PID controller in the next chapter.

4.1 Routh Stability

The requirement for solutions $\phi = \hat{\phi}$ to the reduced Euler-Lagrange equations to be stable is that $d^2V_\mu(\hat{\phi})$ is positive definite [8]. The equation for the second derivative of the amended potential is

$$V_\mu''(\phi) = 2m_b g(a + b + r) \cos \phi + 3am_1 g \cos \phi + m_2 g(a + b) \cos \phi - \frac{\mu^2 C_p''(\phi)}{2C_p^2(\phi)} + \frac{\mu^2 (C_p'(\phi))^2}{C_p^3(\phi)} \quad (4.1)$$

Thus, the reduced system is stable for values $\phi = \hat{\phi}$ such that $V_\mu''(\hat{\phi}) > 0$.

This is a very complicated expression, and is not directly solvable arithmetically. However, a computer simulation (using typical values for the various parameters) will allow for a general idea of the behaviour of the system. The values of the parameters to be used in the simulation

are provided in Table 4.1.

Table 4.1: Simulation Parameter Values

Parameter	Description	Value
m_1	Mass of connecting rod	0 kg
m_2	Mass of ball rod	0 kg
m_b	Mass of flyball	0.2 kg
a	Length of connecting rod	15 cm
b	Length of ball rod extension	10 cm
r	Radius of flyball	2.5 cm
g	Acceleration due to gravity	9.81 ms^{-2}

Estimating a typical value for μ and $\dot{\theta}$ is slightly more involved, as whilst μ is a constant, its actual value is unknown and defined by specific pairings of $\dot{\theta}$ and ϕ . In other words, substituting any combination of ϕ and $\dot{\theta}$ values into the equation for μ will not give a valid result, as the equation relates the two variables whilst they are in a state of constant rotation (i.e. with $\phi = \text{constant}$ and $\dot{\theta} = \text{constant}$).

In order to get around this, the values of the parameters can be estimated and found by 'working backwards'. Firstly, a value for μ is chosen at random, the associated 'critical' angle $\hat{\phi}$ is then found by solving the equation of motion using the chosen value of μ , and finally the associated rotation speed $\hat{\theta}$ may be found by substituting $\hat{\phi}$ into the equation for μ . This method is explained in greater mathematical detail below.

Recall the equation of motion is

$$M\ddot{\phi} + V'_\mu(\phi) = -4a^2c_1 \sin^2 \phi \dot{\phi},$$

by using the assumptions $m_1 = m_2 = 0$ and constant ϕ , and substituting in the value of $V'_\mu(\phi)$, the equation can be simplified to:

$$\frac{\mu^2}{2} \frac{M_b \sin 2\phi}{M_r^2 + 2M_r M_b \sin^2 \phi + M_b^2 \sin^4 \phi} - G \sin \phi = 0 \quad (4.2)$$

where $G = 2m_b g(a + b + r)$. Rewriting the equation purely in terms of $\sin \phi$:

$$\mu^2 \frac{M_b \sin \phi \sqrt{1 - \sin^2 \phi}}{M_r^2 + 2M_r M_b \sin^2 \phi + M_b^2 \sin^4 \phi} = G \sin \phi$$

Now, let $x = \sin\phi$ (for $0 \leq \phi \leq \frac{\pi}{2}$), and introduce the following parameters:

$$A = M_r^2$$

$$B = 2M_r M_b$$

$$C = M_b^2$$

$$D = M_b \mu^2$$

Then the equation becomes

$$\frac{Dx\sqrt{1-x^2}}{A+Bx^2+Cx^4} = Gx \quad (4.3)$$

which may be rewritten as

$$G^2 C^2 x^8 + 2G^2 BCx^6 + (G^2 B^2 + 2G^2 AC)x^4 + (D^2 + 2G^2 AB)x^2 + G^2 A^2 - D^2 = 0. \quad (4.4)$$

This is an eighth-order function of x , and may be solved numerically. The necessary value of x is the root of the equation that lies in the domain $0 \leq x \leq 1$, and then $\hat{\phi} = \sin^{-1} x$. The corresponding governor rotational speed is then found by substituting $\hat{\phi}$ into equation (3.28).

A plot of the LHS of equation 4.4 is given below in Figure 4.1 below. The value of μ used in this simulation was 0.2 and the associated rotational velocity was found to be approximately 8.5 rad/s.

§4.2. Routh Stability

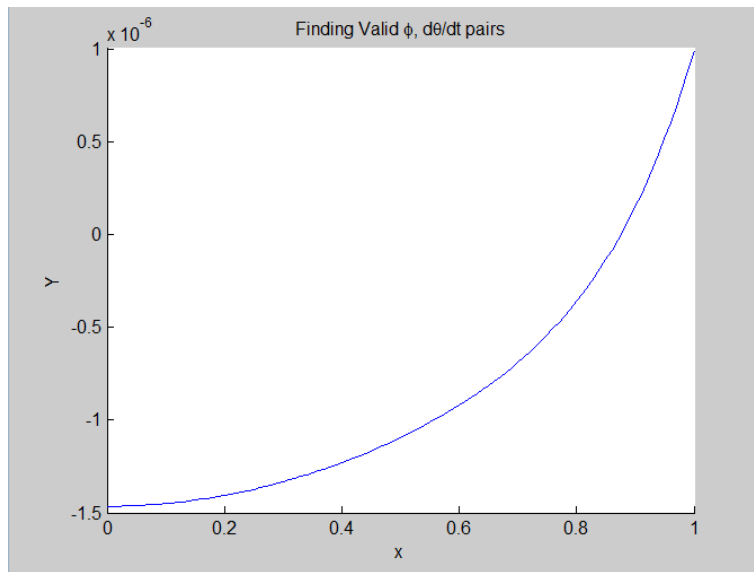


Figure 4.1: Plot of the LHS of Equation (4.4)

An analysis of the general stability behaviour of the system can now be performed, the results of which are presented below in Figure 4.2.

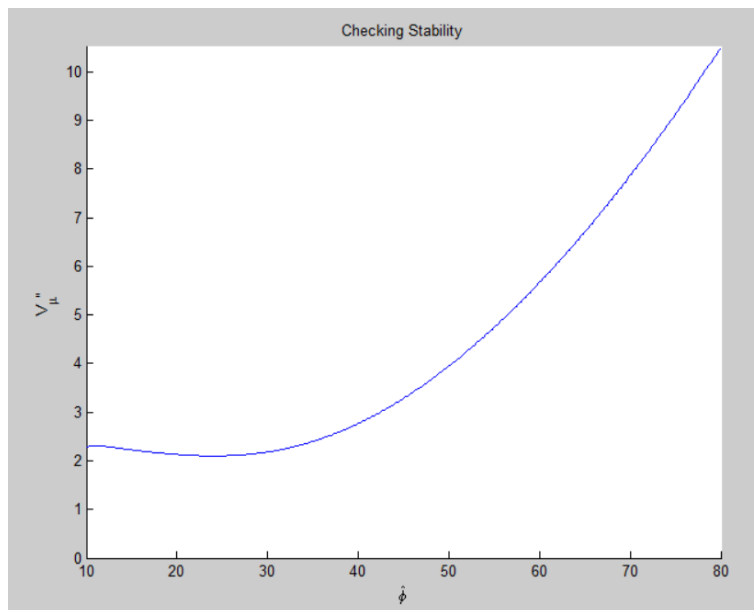


Figure 4.2: Plot of Stability Simulation for Watt Governor

As can be seen from the plot, the value of $V''_{\mu}(\phi)$ is always greater than 0 for the defined domain and thus the system is stable for all values of $\hat{\phi}$ between 10° and 80° .

4.2 Maxwell Stability

Stability criterion for the joint engine-governor system can also be determined by using those derived by Maxwell [9]. These criterion can be used to develop a set of constraints on the parameters of the joint model that will ensure the trajectories are stable given specific operating conditions.

4.2.1 Linearisation

In order to derive the stability criterion, it is necessary to linearise the joint equations of motion. This is done by using the following substitutions

$$\phi = \hat{\phi} + \delta\phi \quad (4.5)$$

$$\omega = \hat{\omega} + \delta\omega \quad (4.6)$$

and assuming the quadratic $\delta\phi$ and $\delta\omega$ terms are negligible. Thus, the linearised equations of motion are:

$$2Mc_3\hat{\omega}^2 \sin \hat{\phi} \cos \hat{\phi} \delta\omega + M(c_3\hat{\omega})^2 \cos 2\hat{\phi} \delta\phi - G \cos \hat{\phi} \delta\phi - \frac{4a^2c_1 \sin^2 \hat{\phi}}{M_r + M_b} \delta\phi = 0 \quad (4.7)$$

$$\delta\dot{\omega} = \frac{K}{I} h'(\hat{\phi}) \delta\phi \quad (4.8)$$

where

$$h'(\hat{\phi}) = \left. \frac{dh}{d\phi} \right|_{\phi=\hat{\phi}}$$

$$M = \frac{M_b}{M_r + M_b}$$

$$G = \frac{M_g}{M_r + M_b}$$

and the masses m_1 and m_2 have again been assumed to be negligible.

Differentiate equation (4.7) with respect to time and substitute in equation (4.8) to get:

$$X\delta\ddot{\phi} + Y\delta\dot{\phi} + Z\delta\phi = 0 \quad (4.9)$$

with coefficients X, Y, Z defined as follows:

$$X = \frac{4a^2c_1 \sin^2 \hat{\phi}}{M_r + M_b} \quad (4.10)$$

$$Y = \frac{G \sin^2 \hat{\phi}}{\cos \hat{\phi}} \quad (4.11)$$

$$Z = -\frac{2KG}{I\hat{\omega}} \sin \hat{\phi} h'(\hat{\phi}) \quad (4.12)$$

4.2.2 Stability

From Maxwell [9], a system is stable if both of the following conditions are true:

$$X, Y, Z > 0 \quad \text{and} \quad XY > Z. \quad (4.13)$$

Given all of the parameters used in this analysis are measurements of physical objects, they must be greater than 0, and so for the first condition to be met, all that is needed is that $h'(\hat{\phi}) < 0$.

The second condition is more complicated, but can be simplified by using Vyshnegradskii's method of introducing a parameter called the nonuniformity of performace as done by Denny [7]. This parameter is defined as:

$$v \equiv \left| \frac{d\hat{\omega}}{d\tau} \right| = \left| \frac{d\hat{\omega}}{d\hat{\phi}} \frac{d\hat{\phi}}{d\tau} \right| \quad (4.14)$$

In this case:

$$v = \frac{\hat{\omega}}{2K|h'(\hat{\phi})|} \frac{\sin^3 \hat{\phi}}{M \sin^2 \hat{\phi} \cos \hat{\phi}} \quad (4.15)$$

And so the second stability condition may be rewritten as

$$s \equiv \frac{4a^2c_1 \sin^2 \hat{\phi} I v}{M_r + M_b} > 1 \quad (4.16)$$

which shows a relationship between the length of the governor arm, the friction of the governor, the initial governor angle, the inertia of the engine, the inertia of the governor and the nonuniformity of performance parameter that must be satisfied for the system to be stable. Similarly to how the model in this paper is more complicated than the model in Denny [7], the stability criterion is also more complicated.

4.3 Transient Response

An examination of the system's response to load disturbance can now be performed by using a simulation of the joint dynamic model developed in the previous chapter. The simulation will be performed using the same parameters that were defined above, as well as the following equilibrium conditions:

$$\begin{aligned}\phi &= \hat{\phi}, \quad \dot{\phi} = 0, \quad \ddot{\phi} = 0 \\ \omega &= \hat{\omega}, \quad \dot{\omega} = 0 \\ \tau &= \hat{\tau}\end{aligned}\tag{4.17}$$

Assuming $h(\phi) = \cos\phi$ and substituting these values into the dynamic equations of motion gives the following two conditions:

$$M_g = M_b(c_3\hat{\omega})^2 \cos \hat{\phi}\tag{4.18}$$

$$K \cos \hat{\phi} = \hat{\tau}\tag{4.19}$$

The exact values of all additional parameters used in this simulation are listed below in Table 4.2. Note that the values of $\hat{\omega}$, $\hat{\tau}$ and $\hat{\phi}$ were chosen, and then equations (4.18) and (4.19) were used to derive c_3 and K . The value of c_1 was chosen such that the system fulfilled the stability criterion developed in the previous section.

Table 4.2: Transient Response Simulation Parameter Values

Parameter	Description	Value
I	Engine Inertia	0.3 kgm ²
c_1	Friction Coefficient	20
c_3	Engine Speed Coefficient	0.2261
K	Engine Fuel Coefficient	141.4
$\hat{\phi}$	Equilibrium Governor Angle	45°
$\hat{\omega}$	Equilibrium Engine Speed	300 rpm
$\hat{\tau}$	Equilibrium Engine Load	100 N

In order to measure the system's response to a load disturbance, an input step function was used for τ , with the value changing from 100N to 95N at time $t = 2s$ 9as shown in Figure 4.3). The reactions of both the governor angle and the engine speed to this change are presented in Figures 4.4 and 4.5 below.

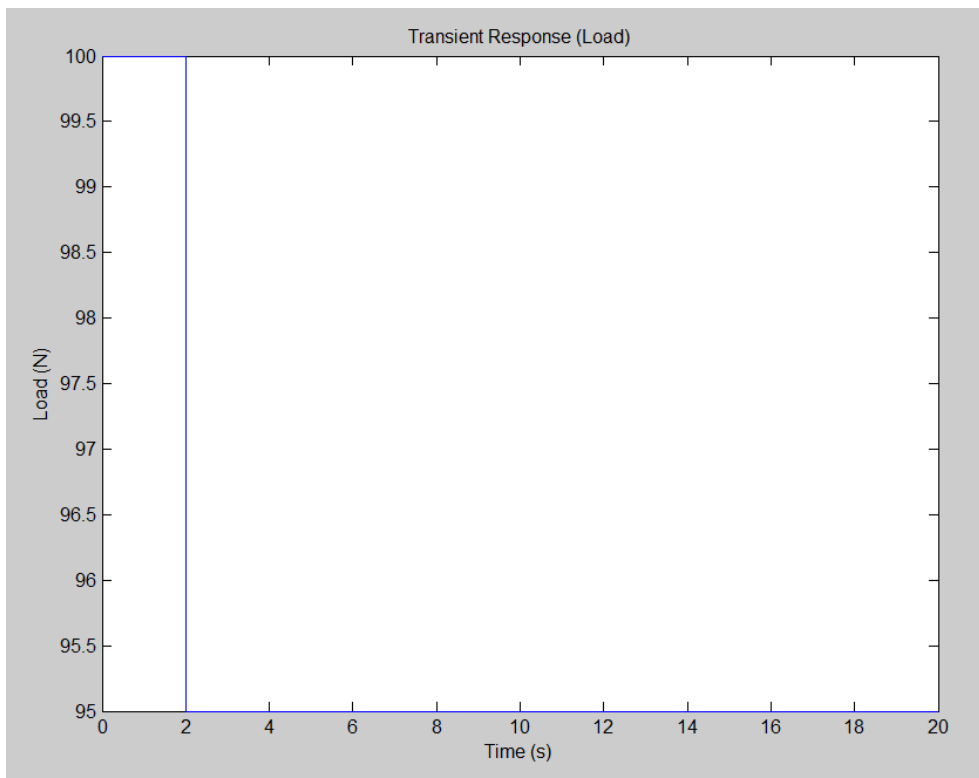


Figure 4.3: Input Step Function ' τ '

§4.3. Transient Response

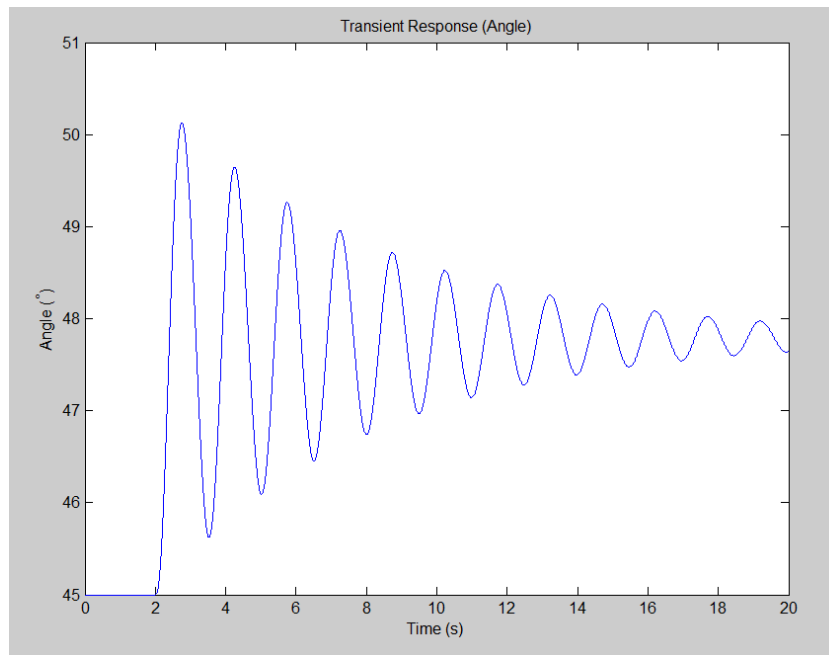


Figure 4.4: Governor Angle Transient Response

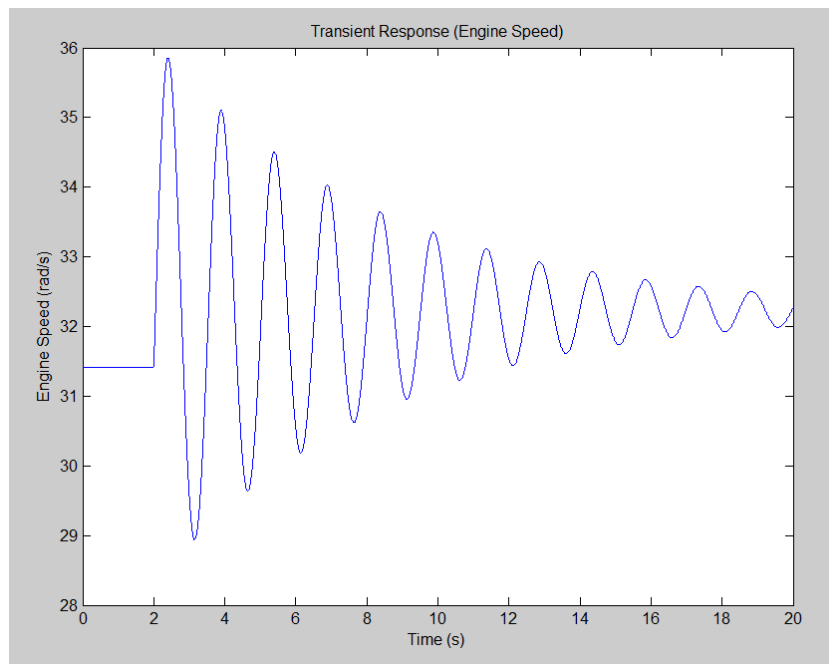


Figure 4.5: Engine Speed Transient Response

These figures clearly show that the system is stable as both the governor angle and the

engine speed both approach a new value. The decrease in the engine load led to an increase in both the governor angle and the engine speed.

These figures also show that the system is underdamped, as the transient response oscillates around the new equilibrium point. The system has a large peak overshoot, a small rise time and a long settling time. Changing the value of the friction coefficient affects these values as seen in Figures 4.6 and 4.7 below where the value of c_1 has been changed to 100.

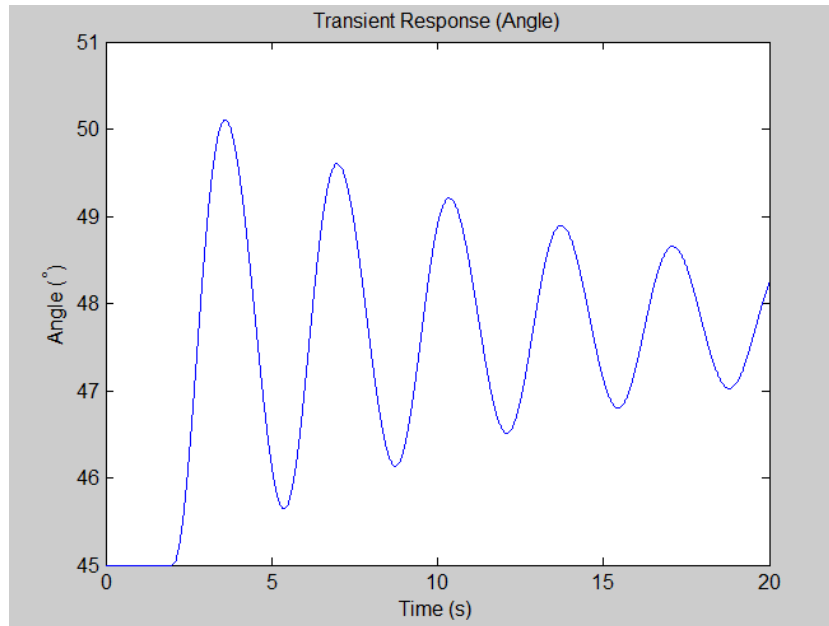


Figure 4.6: Governor Angle Transient Response - Increased Friction Coefficient

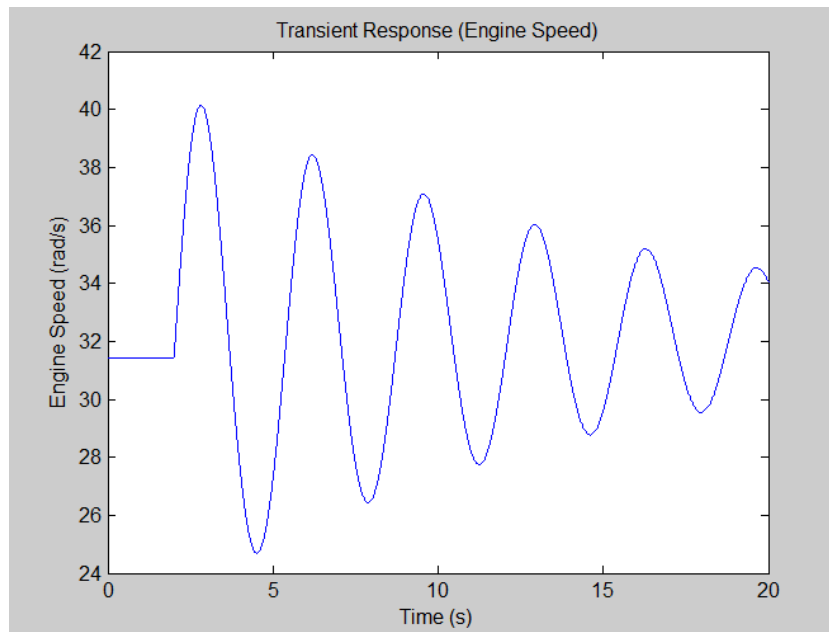


Figure 4.7: Engine Speed Transient Response - Increased Friction Coefficient

It is obvious from these plots that changing the friction coefficient has a large impact on the transient response of the system. Whilst it has no impact on the peak overshoot, increasing c_1 increases both the rise time and the settling, and also the frequency of the oscillations around the new equilibrium point.

Using these values for the parameters, it was not possible to find a value of c_1 that resulted in either the critically damped, or the over-damped case. This implies that either the governor is always underdamped, or that other variables have a further impact on the transient response.

Another interesting observation that can be made about this transient step response is that it appears to be linear in nature, possessing the characteristic exponential envelope, and oscillating at a single frequency. This would suggest that the linear part of the non-linear engine-governor system dominates the step response, and so it may be well approximated by a linear system. In order to investigate the non-linear part of the system, further research would be required, such as examining the system's response to a ramp input.

A Similar Digital Feedback Controller

In this chapter, a PID controller that performed the same control action as the governor is designed and simulated. The controller is developed based on the stability analysis performed in the last chapter, as the damping ratio and the natural frequency of the system is calculated and used to derive the associated transfer function. Analysis of the feedback loop involving the PID controller showed that this controller alone was unable to perform the same action as the governor, and a frictional term had to be added to the engine model. It was then found that the resultant PID controller implemented purely integral control, and thus the governor can be thought of as providing an integral action along with a frictional effect on the engine.

5.1 Joint System Transfer Function

It is impossible to design a linear control mechanism such as a PID controller that is able to implement the same control action as a non-linear system such as the engine-governor interconnection. In such a situation, the PID controller will only be able to implement a control action similar to the linear part of the joint system. However, as discussed in the previous chapter, the step response of the engine-governor system is well approximated as linear, and thus a PID controller that performs a similar action can be designed. To do this, a transfer function that characterises the step response of the engine governor system is generated by first calculating the damping ratio (ζ) and the natural frequency (ω_n) of the system. From [6], the transfer function is given by:

$$H(s) = \frac{\omega_n^2}{s^2 + 2\zeta\omega_n s + \omega_n^2} \quad (5.1)$$

This transfer function then acts as a linearisation of a specific trajectory of the system.

The values for the damping ratio and natural frequency can both be determined from the plots generated in the stability analysis performed in the previous chapter using a method from [6]. An annotated plot of the transient response for the engine speed is shown below in Figure 5.1, using the default parameter values.

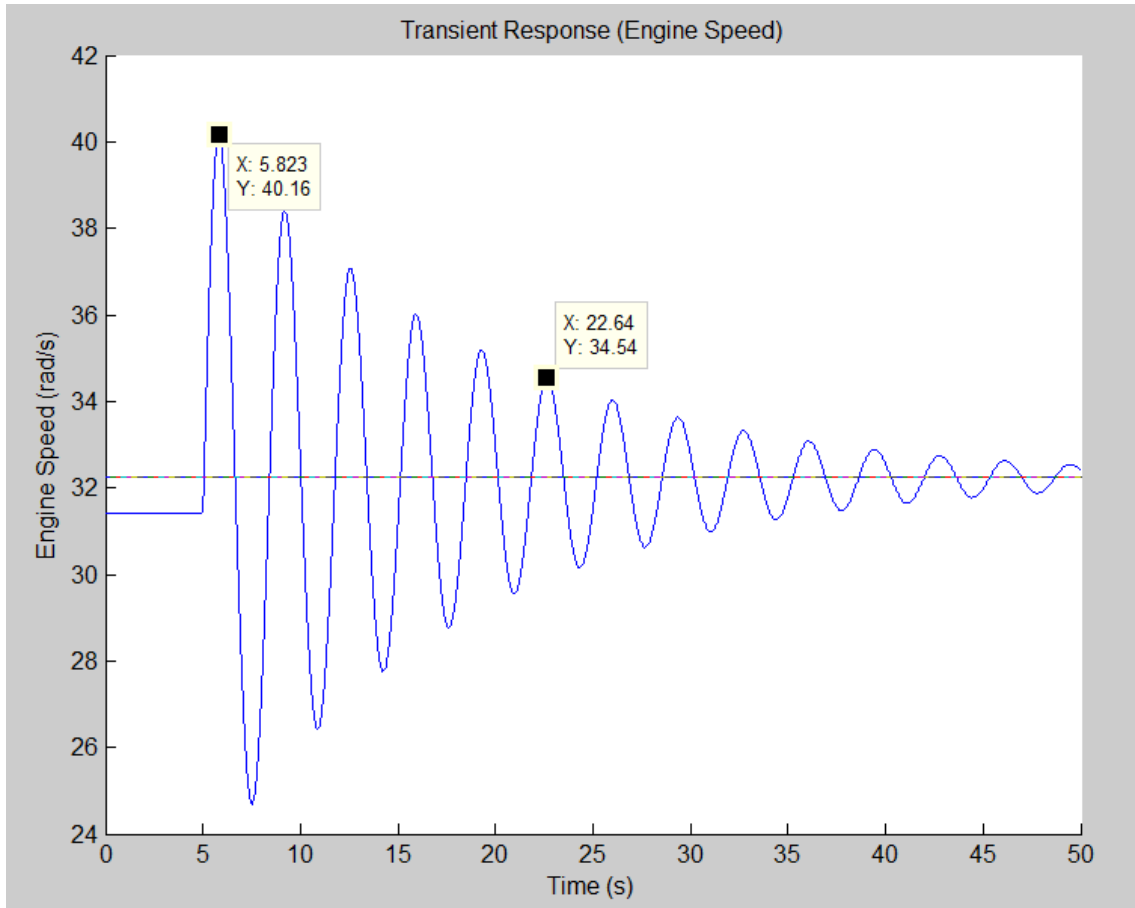


Figure 5.1: Annotated Engine Speed Transient Response Plot

The two points marked on the plot are the first peak (called $x(t_0)$), and the sixth peak (called $x(t_5)$). The time between the two points ($t_5 - t_0$) represents five periods of the function's oscillation, and thus one period (T_d) is equivalent to:

$$T_d = \frac{t_5 - t_0}{5} \quad (5.2)$$

The damped frequency (ω_d) of the system is can then be calculated using the equation:

$$\omega_d = \frac{2\pi}{T_d} \quad (5.3)$$

The logarithmic decrement (LD) of the system is a measure of how quickly the system approaches its final value, and is defined by the following ratio:

$$LD = \frac{x(t_5) - x(\infty)}{x(t_0) - x(\infty)} \quad (5.4)$$

where $x(\infty)$ is the limiting value that the function approaches, in this case, this was found to be $x(\infty) = 32.25\text{rad/s}$.

Knowing that the system is underdamped and the damping ratio is small, it is therefore given by:

$$\zeta = -\frac{1}{2\pi k} \ln(LD) \quad (5.5)$$

where k is the number of periods between t_0 and t_5 , which in this case is equal to five.

Finally, the natural frequency of the system is related to the damped frequency and the damping ratio, and may be calculated using:

$$\omega_n = \frac{\omega_d}{\sqrt{1 - \zeta^2}} \quad (5.6)$$

Substituting the values from the plot into this series of equations results in the transfer function for the engine-governor system. which was calculated as:

$$H(s) = \frac{3.5}{s^2 + 0.15s + 3.5} \quad (5.7)$$

5.1.1 Further Governor Design

Damping ratio and natural frequency are both important values when it comes to designing a control system, as they are directly related to the rise time (t_r), the percent overshoot (M_p), and the settling time (t_s) of the system. The relationships between these values is

defined in [6] and are given below:

$$t_r \approx \frac{1.8}{\omega_n} \quad (5.8)$$

$$M_p = e^{-\pi\zeta/\sqrt{1-\zeta^2}}, \quad 0 \leq \zeta < 1 \quad (5.9)$$

$$t_s = \frac{4.6}{\zeta\omega_n} \quad (5.10)$$

It can be seen from these relationships that if ζ increases, then t_s and M_p will decrease, whilst if ω_n increases, both t_r and t_s will decrease.

A brief investigation into the effects of varying system parameters on the damping ratio and natural frequency was performed in order to try and develop some basic guidelines for governor design. The tests were performed by changing the values of the parameters used in the simulation, and then repeating the derivation given above. The results are summarised below in Table 5.1.

Table 5.1: Effect of Varying Parameters on Damping Ratio and Natural Frequency

Variation	Damping Ratio (ζ)	Natural Frequency (ω_n)
None	0.039	1.87
Governor Arm Length (a) $\times 2$	0.025	1.15
a $\times 0.5$	0.058	3.20
Flyball Mass (m_b) $\times 2$	0.048	2.65
$m_b \times 0.5$	0.030	1.32
Governor Arm Extension (b) $\times 2$	0.040	2.18
b $\times 0.5$	0.037	1.69
b $\times 0$	0.034	1.49
Flyball Radius (r) $\times 2$	0.040	1.95
r $\times 0.5$	0.039	1.83
Governor Friction Coefficient (c_1) $\times 2$	0.030	0.93
$c_1 \times 0.5$	0.048	2.65

As can be seen from the table, varying either the length of the governor arm, or the mass of

the flyball leads to a large change in both the damping ratio and the natural frequency, whilst changing the flyball radius or the length of the extension has minimal impact. Additionally, a decrease in the arm length leads to an increase in the two measured values, which in turn will lead to a decrease in the rise time, the percent overshoot and the settling time of the system. Similarly, an increase in the flyball mass, and a decrease in the friction coefficient will also lead to a decrease in the three design parameters.

5.2 PID Controller

5.2.1 Transfer Function Derivation

Block Diagram

The type of digital feedback controller used to mimic the action of the governor was the PID controller, given that it is the most common type of digital controller currently in use. The implementation of this controller was done within a simple negative unity feedback loop, as shown in the block diagram below in Figure 5.2.

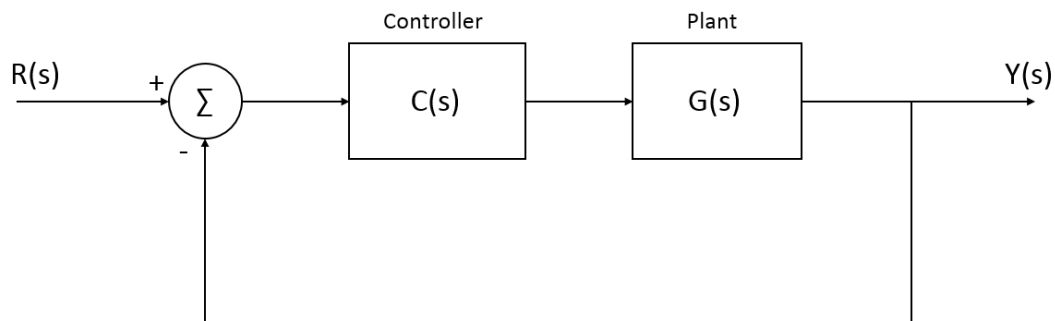


Figure 5.2: Digital Feedback Controller Block Diagram

Using simple block diagram arithmetic, the closed loop transfer function for the system is:

$$H_{PID}(s) = \frac{C(s)G(s)}{1 + C(s)G(s)} \quad (5.11)$$

The transfer function of a PID controller is given in [6] as:

$$C(s) = k_p + \frac{k_i}{s} + k_d s, \quad (5.12)$$

where k_p is the proportional term, k_i is the integral term and k_d is the derivative term. The transfer function for the plant, which in this case is the engine, is:

$$G(s) = \frac{K}{Is} \quad (5.13)$$

where K is a constant relating the input variable with engine torque, and I is the engine moment of inertia.

Substituting equations (5.12) and (5.13) into equation (5.11) gives the transfer function for the system:

$$\begin{aligned} H_{PID}(s) &= \frac{\frac{K}{Is}(k_p + \frac{k_i}{s} + k_d s)}{1 + \frac{K}{Is}(k_p + \frac{k_i}{s} + k_d s)} \\ &= \frac{Kk_d s^2 + Kk_p s + Kk_i}{(Kk_d + I)s^2 + Kk_p s + Kk_i} \end{aligned} \quad (5.14)$$

Equating Coefficients

In order to copy the control action of the governor, the transfer function for the feedback control loop must be the same as the one for the engine-governor system. Thus, the two can be equated, and this may be used to solve for the values of k_p , k_i and k_d . Dividing both the numerator and denominator of equation (5.14) by $(Kk_d + I)$ and then equating this with equation (5.1) gives the following result:

$$\frac{\frac{Kk_d}{Kk_d+I}s^2 + \frac{Kk_p}{Kk_d+I}s + \frac{Kk_i}{Kk_d+I}}{s^2 + \frac{Kk_p}{Kk_d+I}s + \frac{Kk_i}{Kk_d+I}} = \frac{\omega_n^2}{s^2 + 2\zeta\omega_n s + \omega_n^2} \quad (5.15)$$

The coefficients of all powers of s in both the numerator and the denominator can then be equated to give five conditions that need to be satisfied.

$$\frac{Kk_d}{Kk_d + I} = 0 \quad (5.16)$$

$$\frac{Kk_p}{Kk_d + I} = 0 \quad (5.17)$$

$$\frac{Kk_i}{Kk_d + I} = \omega_n^2 \quad (5.18)$$

$$\frac{Kk_p}{Kk_d + I} = 2\zeta\omega_n \quad (5.19)$$

$$\frac{Kk_i}{Kk_d + I} = \omega_n^2 \quad (5.20)$$

Condition (5.16) implies $k_d = 0$; condition (5.17) implies $k_p = 0$; condition (5.18) implies $k_i = \frac{\omega_n^2 I}{K}$; condition (5.19) implies $k_p = \frac{2\zeta\omega_n I}{K}$ and condition (5.20) is the same as condition (5.18).

Thus there is a contradiction, as one condition implies k_p is zero, whilst another implies it is non-zero, and so it can be seen that a PID controller is unable to mimic the control action of the governor in this setup.

Frictional Term

This problem may be overcome by introducing a friction term into the engine model. The friction term acts against the motion of the engine, and is proportional to the engine velocity with friction coefficient f_{eng} , thus the transfer function for the engine becomes:

$$G(s) = \frac{K}{Is + f_{eng}} \quad (5.21)$$

Substituting this into equation (5.14) results in an updated transfer equation for the overall system

$$H_{PID}(s) = \frac{Kk_d s^2 + Kk_p s + Kk_i}{(Kk_d + I)s^2 + (Kk_p + f_{eng})s + Kk_i} \quad (5.22)$$

Dividing both sides by $(Kk_d + I)$ and equating it with equation (5.1) gives a new set of five conditions:

$$\frac{Kk_d}{Kk_d + I} = 0 \quad (5.23)$$

$$\frac{Kk_p}{Kk_d + I} = 0 \quad (5.24)$$

$$\frac{Kk_i}{Kk_d + I} = \omega_n^2 \quad (5.25)$$

$$\frac{Kk_p + f_{eng}}{Kk_d + I} = 2\zeta\omega_n \quad (5.26)$$

$$\frac{Kk_i}{Kk_d + I} = \omega_n^2 \quad (5.27)$$

It is immediately obvious that the only condition that has changed is condition (5.26), and that it is no longer contradictory with condition (5.24). Indeed, if $k_p = k_d = 0$, then condition (5.26) implies $f_{eng} = 2\zeta\omega_n I$.

Therefore, a PID controller of the form

$$C(s) = \frac{I\omega_n^2}{Ks} \quad (5.28)$$

is able to implement the same control action as the governor, with the additional constraint that the engine friction coefficient is

$$f_{eng} = 2I\zeta\omega_n \quad (5.29)$$

In the joint engine-governor interconnection, the friction within the engine would be provided by the friction within the governor, which explains why the first engine model was valid as part of the joint engine-governor system.

5.2.2 Comparison with Governor

To compare the control action of this PID controller with that of the governor, a simulation was created using Simulink to visualise the transient response. Figure 5.3 shows the results of this simulation along with the results of a similar simulation using the governor model for comparison.

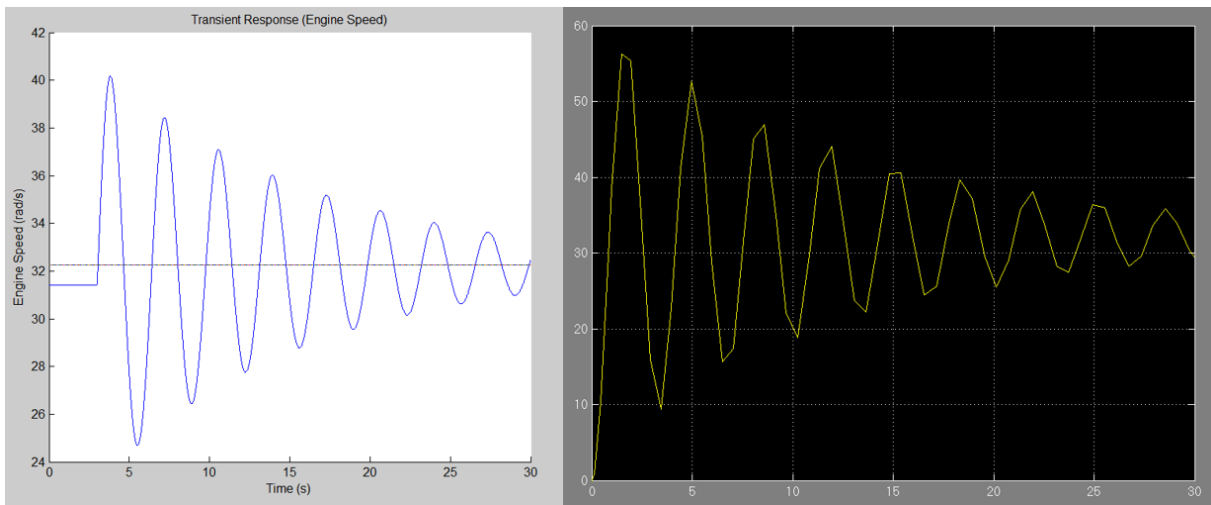


Figure 5.3: Engine Speed Transient Response using Governor Model (left) and PID Controller Model (right)

Inspection of both plots shows that the transient response for both models appears to be the same, as they have the same overall shape. The major similarities are that they have the same rise time and settling time (note that governor model is slightly delayed due to the step occurring later than in the PID model). However, the value of the percent overshoot is greater in the PID model than in the governor model. Two possible causes for this inconsistency are that the simulink model uses an initial value of zero rather than 31.4 in the governor model; or that the derivation of the PID model transfer function is based off a unit step response, whereas the governor model uses a non-unity step, which may have led to scaling issues.

Thus, we can see that the flyball governor provides an integral control action, as well as providing a frictional force upon the engine. This results in a very complicated relationship as the value of the frictional force is actually dependent on the velocity of the governor.

Conclusion

As a result of the analysis performed in this paper, a number of conclusions can be drawn:

- In this case, combining the two models before performing Routh reduction gives the same result as combining the models after performing Routh reduction on them separately;
- The Watt governor is stable for all possible parameter combinations
- The joint engine-governor system is stable given both $\frac{4a^2c_1 \sin^2 \hat{\phi} I v}{M_r + M_b} > 1$ and $h'(\hat{\phi}) < 0$ are satisfied;
- The engine-governor system is always-underdamped;
- The governor provides both an integral control action and a frictional force as its method of control.

6.1 Further Work

Further research that could be done in this area would be to further investigate the stability criteria and transient response of the governor to develop a rigorous set of governor design principles. Another possible area would be to focus on the relationship between the governor and the PID controller to determine the exact relationship between the governor parameters and the PID coefficients. Additionally, work could also be done in investigating other types of governors, and to see how the stability analysis or transient response is affected by the different governor designs.

Bibliography

1. R. L. Hills, *Power from wind: a history of windmill technology*. Cambridge University Press, 1996. (cited on page 2)
2. C. Sharma and K. Purohit, *Theory of Mechanisms and Machines*. PHI Learning Pvt. Ltd., 2006. (cited on pages 2, 3, 4, 5, and 6)
3. L. Derr, *Cyclopedia of Engineering*. American Technical Society, 1911. (cited on page 4)
4. (2014) Proell governor, gravity controlled centrifugal governors, assignment help. Accessed: 04-08-2014. [Online]. Available: <http://www.expertsmind.com/topic/gravity-controlled-centrifugal-governors/proell-governor-98985.aspx> (cited on page 5)
5. (2014) Hartnell governor, spring controlled centrifugal governors, assignment help. Accessed: 04-08-2014. [Online]. Available: <http://www.expertsmind.com/topic/spring-controlled-centrifugal-governors/hartnell-governor-98987.aspx> (cited on page 6)
6. G. F. Franklin, J. D. Powell, A. Emami-Naeini, and J. D. Powell, *Feedback control of dynamic systems*. Addison-Wesley Reading, 1994, vol. 3. (cited on pages 6, 8, 40, 41, 43, and 45)
7. M. Denny, "Watt steam governor stability," *European Journal of Physics*, vol. 23, no. 3, p. 339, 2002. (cited on pages 7, 22, 34, and 35)
8. J. E. Marsden and T. Ratiu, *Introduction to mechanics and symmetry: a basic exposition of classical mechanical systems*. Springer Science & Business Media, 2013, vol. 17. (cited on pages 7, 19, and 29)
9. J. C. Maxwell, "On governors," *Proceedings of the Royal Society of London*, vol. 16, pp. 270–283, 1867. (cited on pages 7, 33, and 34)
10. K. J. Aström and R. M. Murray, *Feedback systems: an introduction for scientists and engineers*. Princeton university press, 2010. (cited on page 8)

§.0. BIBLIOGRAPHY

11. M. Araki, "Pid control," *Control systems, robotics and automation*, vol. 2, pp. 1–23, 2002.
(cited on page 8)
12. N. C. Rana and P. S. Joag, *Classical mechanics*. Tata McGraw-Hill Publishing Company, 1991. (cited on page 9)

Appendices

A.1 Variables in their Expanded Forms

$$C_p(\phi) = \frac{4m_b r^2}{5} + 2m_b(a+b+r)^2 \sin^2 \phi + \frac{2}{3}m_1 a^2 \sin^2 \phi + \frac{2}{3}m_2(a+b)^2 \sin^2 \phi$$

$$C'_p(\phi) = 2m_b(a+b+r)^2 \sin 2\phi + \frac{2}{3}m_1 a^2 \sin 2\phi + \frac{2}{3}m_2(a+b)^2 \sin 2\phi$$

$$C''_p(\phi) = 4m_b(a+b+r)^2 \cos 2\phi + \frac{4}{3}m_1 a^2 \cos 2\phi + \frac{4}{3}m_2(a+b)^2 \cos 2\phi$$

$$V_\mu(\phi) = 2m_b g(a+b+r) - 2m_b g(a+b+r) \cos \phi + 3am_1 g - 3am_1 g \cos \phi + m_2 g(a+b) \\ - m_2 g(a+b) \cos \phi + \frac{\mu^2}{2} \frac{1}{\frac{4m_b r^2}{5} + 2m_b(a+b+r)^2 \sin^2 \phi + \frac{2}{3}m_1 a^2 \sin^2 \phi + \frac{2}{3}m_2(a+b)^2 \sin^2 \phi}$$

$$V'_\mu(\phi) = 2m_b g(a+b+r) \sin \phi + 3am_1 g \sin \phi + m_2 g(a+b) \sin \phi \\ - \frac{\mu^2}{2} \frac{2m_b(a+b+r)^2 \sin 2\phi + \frac{2}{3}m_1 a^2 \sin 2\phi + \frac{2}{3}m_2(a+b)^2 \sin 2\phi}{\left(\frac{4m_b r^2}{5} + 2m_b(a+b+r)^2 \sin^2 \phi + \frac{2}{3}m_1 a^2 \sin^2 \phi + \frac{2}{3}m_2(a+b)^2 \sin^2 \phi\right)^2}$$

$$V''_\mu(\phi) = 2m_b g(a+b+r) \cos \phi + 3am_1 g \cos \phi + m_2 g(a+b) \cos \phi \\ - \frac{\mu^2}{2} \frac{4m_b(a+b+r)^2 \cos 2\phi + \frac{4}{3}m_1 a^2 \cos 2\phi + \frac{4}{3}m_2(a+b)^2 \cos 2\phi}{\left(\frac{4m_b r^2}{5} + 2m_b(a+b+r)^2 \sin^2 \phi + \frac{2}{3}m_1 a^2 \sin^2 \phi + \frac{2}{3}m_2(a+b)^2 \sin^2 \phi\right)^2} \\ + \mu^2 \frac{(2m_b(a+b+r)^2 \sin 2\phi + \frac{2}{3}m_1 a^2 \sin 2\phi + \frac{2}{3}m_2(a+b)^2 \sin 2\phi)^2}{\left(\frac{4m_b r^2}{5} + 2m_b(a+b+r)^2 \sin^2 \phi + \frac{2}{3}m_1 a^2 \sin^2 \phi + \frac{2}{3}m_2(a+b)^2 \sin^2 \phi\right)^3}$$

A.2 Governor Design

Velocity Profile Diagrams

In the figures below, the blue line represents the default case, the red line represents the case where the parameter has been doubled, the green line represents the case where the parameter has been halved and the magenta line represents an extraordinary case (e.g. the parameter has been set to 0).

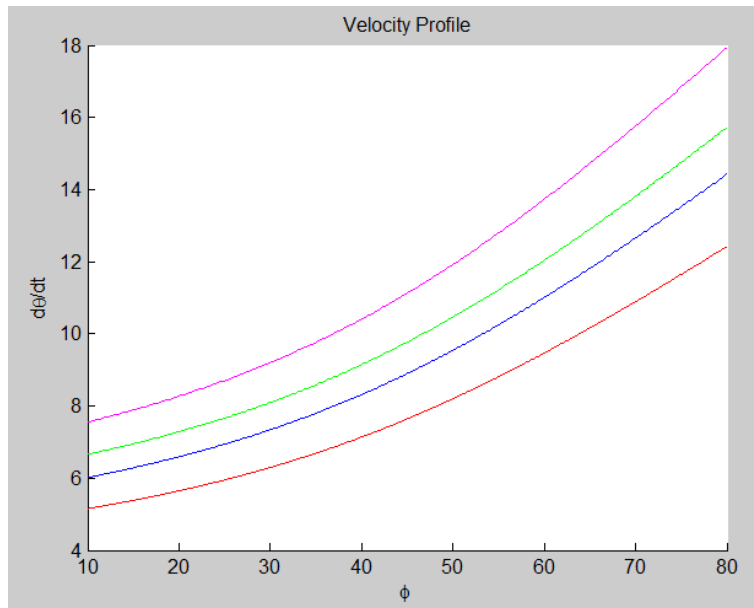


Figure A.1: Velocity Profile - Changing Governor Arm Extension

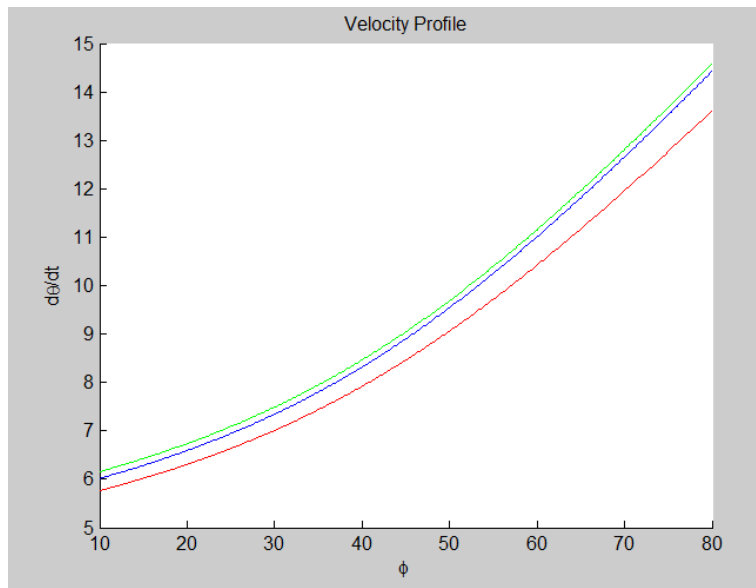


Figure A.2: Velocity Profile - Changing Flyball Radius

Velocity Graphs

The graphs below show how specific points change as each of the parameters are changed individually. The points examined were the 'minimum' point (the velocity at $\phi = 10^\circ$, represented by an orange line), the 'operating' point (the velocity at $\phi = 45^\circ$, represented by a gray line) and the 'maximum' point (the velocity at $\phi = 80^\circ$, represented by a blue line).

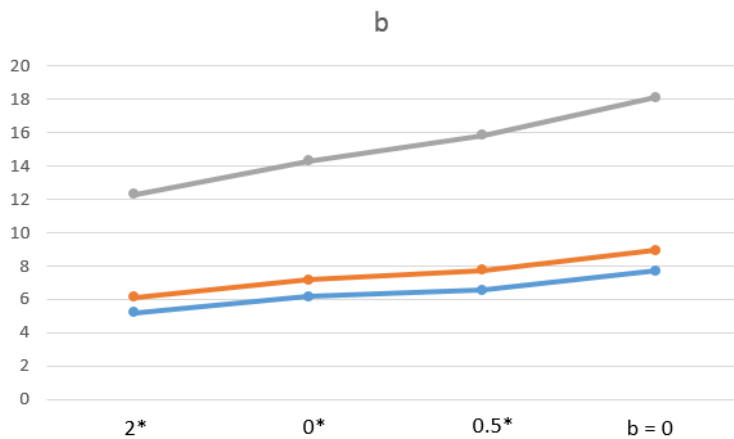


Figure A.3: Velocity Graph - Changing Governor Arm Extension

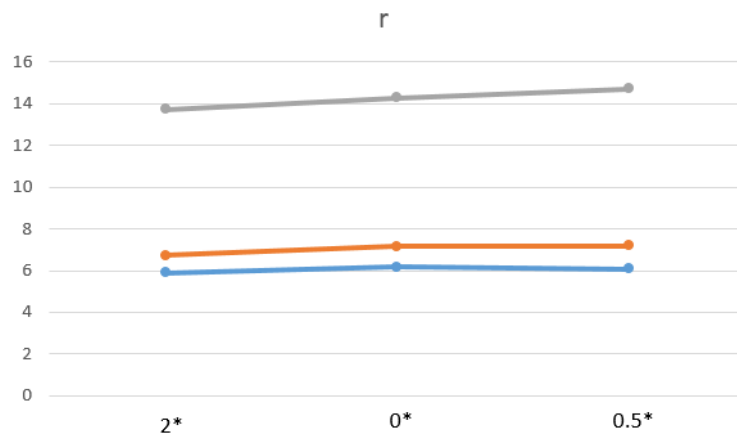


Figure A.4: Velocity Graph - Changing Flyball Radius

Modification of Governor Arm Length and Governor Arm Extension in Combination

In the figures below, the blue line represents the default case, the red line represents the case where only governor arm length ('a') has been modified, the green line represents the case where only governor arm extension ('b') has been modified and the magenta line represents the case where both parameters have been modified.

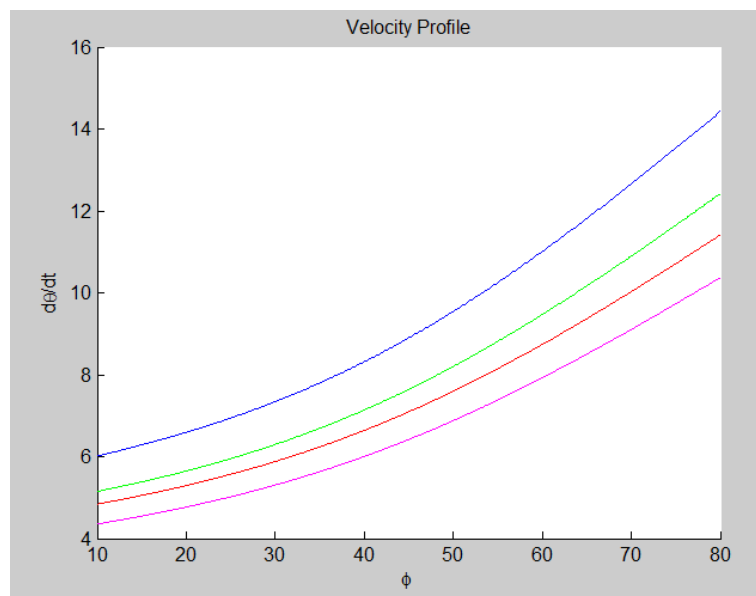


Figure A.5: Velocity Profile - Combining 2*'a' and 2*'b'

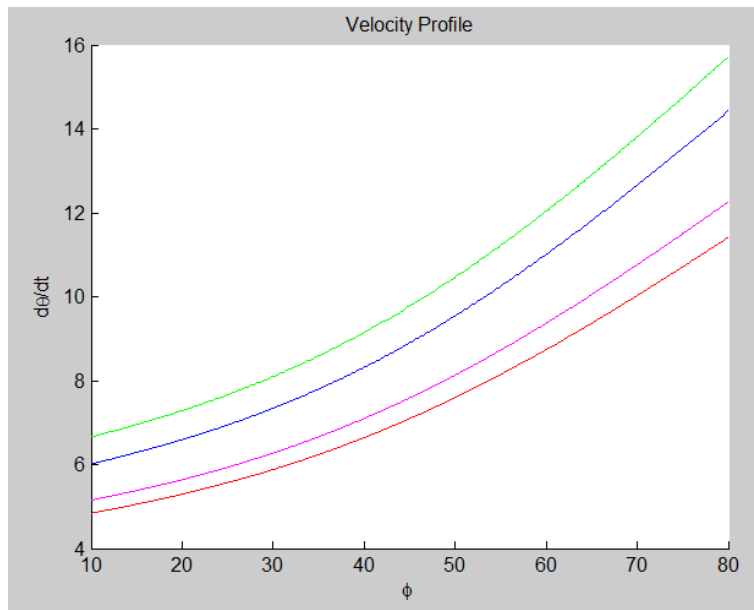


Figure A.6: Velocity Profile - Combining $2 \cdot a'$ and $1/2 \cdot b'$

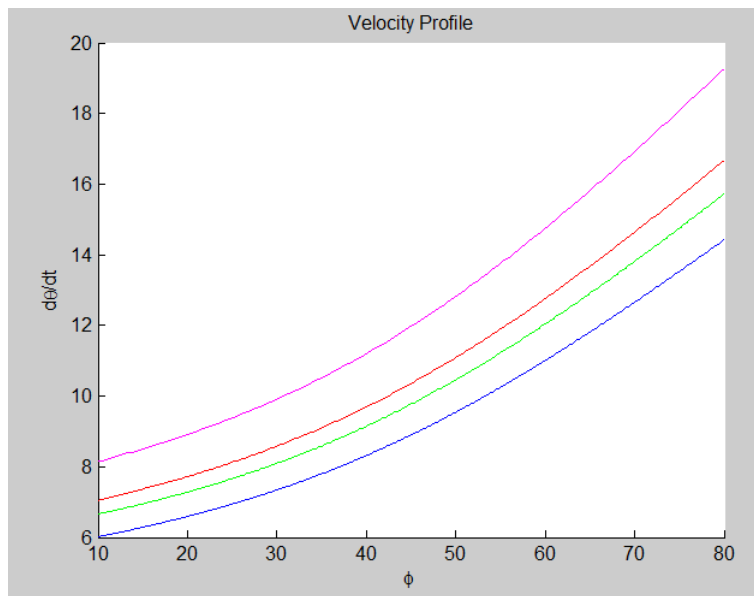


Figure A.7: Velocity Profile - Combining $1/2 \cdot a'$ and $1/2 \cdot b'$

These figures show that the parameters 'a' and 'b' do not combine additively, e.g. the shift in the profile induced by doubling 'a' and doubling 'b' is not equal to the sum of the shift of the profile induced by doubling 'a' and the shift in the profile induced by doubling

'b' individually. This means that the velocity function is not a linear combination of 'a' and 'b' and so is inversely related to 'ab' in some manner.

The graph below (Figure A.8) shows the impact of the 'a' and 'b' terms being applied together to the 'minimum', 'maximum' and 'operating' point values, and shows that the dependence on 'ab' is likely to be linear. It also shows that the effect of 'a' and 'b' together is very similar to the effect of 'a' and 'b' individually from a behavioural perspective, as there is a larger effect on the 'maximum' point then on the 'minimum' point.

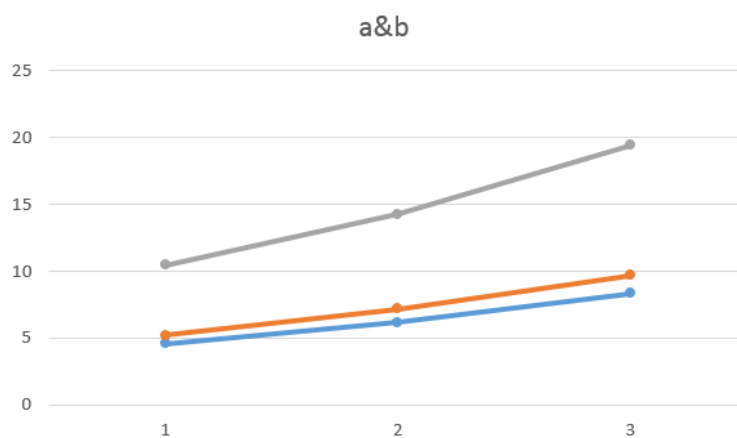


Figure A.8: Velocity Graph - Changing 'a' & 'b'

A.3 Matlab Code

stab_plot.m

```

1
2 close all
3 clear all
4 hold on
5
6 % define parameters (can vary)
7 m = 0.2; %kg
8 m1 = 0.01; %kg
9 m2 = m1; %kg

```

§A.3. Matlab Code

```

10 a = 0.15; %metres
11 r = 0.025; %m
12 b = 0.1; %m
13 g = 9.81; %m/s^2
14 Y = [];
15 x = 0:0.01:1;
16 mu = 0.11; %used to find crit angles and velocities
17
18 % derived parameters
19 Mr = 4/5 * m * r^2;
20 Mb = 2 * m * (a+b+r)^2;
21 M1 = 8/3 * m1 * a^2;
22 M2 = 8/3 * m2 * (a+b)^2;
23 G = (2 * m * g * (a+b+r)) + (3 * a * m1 * g) + (m2 * g * (a+b));
24 D = (Mb + M1 + M2) * mu^2 ;
25 A = Mr^2;
26 B = 2 * Mr * (Mb + M1 + M2);
27 C = (Mb + M1 + M2)^2;
28
29 % solve for phi
30 y = 10000;
31 n = 0;
32
33 for i = 1:length(x)
34
35     y = G^2*C^2*x(i)^8 + 2*G^2*B*C*x(i)^6 + (G^2*B^2 + 2*G^2*A*C)*x(i)^4 + ...
36         (D^2 + 2*G^2*A*B)*x(i)^2 + (G^2*A^2 - D^2);
37     Y = [Y y];
38
39 end
40
41 syms p
42
43 f = G^2*C^2*p^8 + 2*G^2*B*C*p^6 + (G^2*B^2 + 2*G^2*A*C)*p^4 + ...
44     (D^2 + 2*G^2*A*B)*p^2 + (G^2*A^2 - D^2);
45
46 k = vpasolve(f, p, [0 1]);
47 l = asin(k);

```

```

48 q = mu/ (Mr + (Mb + M1 + M2) * (sin(l))^2);
49
50 % solve for phi
51 phi = asin(x(n)); %radians
52
53 % solve for theta dot
54 o = mu/ (Mr + (Mb + M1 + M2) * (sin(phi))^2);
55
56 % disp data and plot
57 disp('crit angle')
58 disp((phi*180/pi))
59 disp('engine speed')
60 disp(o)
61
62 plot(x,Y)
63 xlabel('x')
64 ylabel('Y')
65 title('Finding Valid \phi, d\theta/dt pairs')
66
67
68 %% plot velocity profile
69
70
71 %figure
72 O = [];
73 Q = [];
74 mu1 = 0.0034; %varies
75 mu2 = 0.24; %varies
76
77 for mu = mu1:0.001:mu2
78     % solve for phi
79     y = 10000;
80     n = 0;
81     D = (Mb + M1 + M2) * mu^2 ;
82
83     syms p
84
85     f = G^2*C^2*p^8 + 2*G^2*B*C*p^6 + (G^2*B^2 + 2*G^2*A*C)*p^4 + ...

```

```

86         (D^2 + 2*G^2*A*B)*p^2 + (G^2*A^2 - D^2);
87
88     k = vpasolve(f, p, [0 1]);
89     phi = asin(k);
90
91     % solve for theta dot
92     o = mu/ (Mr + (Mb + M1 + M2) * (sin(phi))^2);
93     O = [0 o];
94 end
95
96 phiv = linspace(10,80,length(O));
97 plot(phiv,0,'g')
98 xlabel('\phi')
99 ylabel('d\theta/dt')
100 title('Velocity Profile')
101
102
103
104
105 %% checking stability
106
107 V = [];
108 mu_vec = 0.006:0.001:0.425;
109
110 for i = 1:length(mu_vec)
111
112     % derived parameters
113     D = (Mb + M1 + M2) * mu_vec(i)^2 ;
114
115     % solve for phi and find theta
116     syms p
117
118     f = G^2*C^2*p^8 + 2*G^2*B*C*p^6 + (G^2*B^2 + 2*G^2*A*C)*p^4 + ...
119         (D^2 + 2*G^2*A*B)*p^2 + (G^2*A^2 - D^2);
120
121     k = vpasolve(f, p, [0 1]);
122     phi = asin(k);
123     o = mu/ (Mr + (Mb + M1 + M2) * (sin(phi))^2);

```

```

124
125     Cp = Mr + (Mb + M1 + M2) * (sin(phi))^2;
126     dCp = (Mb + M1 + M2) * sin(2*(phi));
127     d2Cp = 2 * (Mb + M1 + M2) * cos(2*(phi));
128
129     % define V
130     v = G * cos(phi) - (mu_vec(i)^2 * d2Cp)/(2 * Cp^2) + mu_vec(i)^2 ...
131         * (dCp^2)/(Cp^3);
132     V = [V v];
133
134 end
135
136 phi_crit = linspace(10,80,length(V));
137
138 % plot results
139
140 plot(phi_crit,V)
141 xlabel('\hat{\phi}','Interpreter','Latex')
142 ylabel('V_\mu')
143 title('Checking Stability')
144 axis([10 80 0 inf])

```

stab_sim.m

```

1
2 close all
3 clear all
4
5 % define parameters
6 m = 0.2; %kg
7 m1 = 0.00; %kg
8 m2 = m1; %kg
9 a = 0.15; %metres
10 r = 0.025; %m
11 b = 0.1; %m
12 g = 9.81; %m/s^2
13 I = 0.3; %kgm^2

```

§A.3. Matlab Code

```
14 c1 = 100;
15
16 % derived parameters
17 Mr = 4/5 * m * r^2;
18 Mb = 2 * m * (a+b+r)^2;
19 M1 = 8/3 * m1 * a^2;
20 M2 = 8/3 * m2 * (a+b)^2;
21 G = (2 * m * g * (a+b+r)) + (3 * a * m1 * g) + (m2 * g * (a+b));
22 A = Mr^2;
23 B = 2 * Mr * (Mb + M1 + M2);
24 C = (Mb + M1 + M2)^2;
25
26 % steady-state values
27 w = 300 * 2 * pi / 60; %(rpm)
28 phi = 45 * pi / 180; %rads
29 T = 100; %N
30 c3 = sqrt(G/(Mb * cos(phi) * w^2));
31 K = T/cos(phi);
32
33 X = (4 * a^2 * c1 * (sin(phi))^2)/(Mr + Mb);
34 Y = (G/(Mr + Mb)) * ((sin(phi))^2 / cos(phi));
35 Z = - (2 * G * K * sin(phi) * (-sin(phi)))/((Mr + Mb) * I * w);
36 disp('stability, true = 1')
37 disp(X*Y > Z)
38
39 %% explicit Euler solution of ode
40
41 % define initial values
42 dt = 0.001;
43 t = 0:dt:30;
44 w0 = w;
45 phi0 = phi;
46 T0 = T;
47
48 % initialise vectors
49 p = zeros(1, length(t));
50 p1 = zeros(1, length(t));
51 p2 = zeros(1, length(t));
```

```

52 o = zeros(1, length(t));
53 o1 = zeros(1, length(t));
54 tau = zeros(1, length(t));
55 p(1) = phi0;
56 o(1) = w0;
57 tau(1) = T0;
58
59 flag = 0;
60 peak1 = o(1);
61 peak2 = o(1);
62 low1 = o(1);
63 peak1t = 0;
64 peak2t = 0;
65 low1t = 0;
66
67 % solve using explicit euler method
68 for i = 1:length(t)-1
69     p(i+1) = p(i) + dt * p1(i);
70     p1(i+1) = p1(i) + dt * p2(i);
71     p2(i+1) = (c3^2 * o(i)^2 * Mb * sin(p(i)) * cos(p(i)))/(Mr + Mb) ...
72         - (G * sin(p(i)))/(Mr + Mb) ...
73         - (4 * a^2 * c1 * (sin(p(i)))^2 * p1(i))/(Mr + Mb);
74     o(i+1) = o(i) + dt * o1(i);
75     o1(i+1) = K * cos(p(i)) / I - tau(i)/I;
76     if i == floor(length(t)/10)
77         tau(i+1) = 95;
78     else
79         tau(i+1) = tau(i);
80     end
81
82     if flag == 0
83         if o(i+1) ≥ peak1
84             peak1 = o(i+1);
85             peak1t = i+1;
86             low1 = peak1;
87         else
88             flag = 1;
89         end

```

```
90     elseif i > peak1t && flag == 1
91         if o(i+1) ≤ low1
92             low1 = o(i+1);
93             low1t = i;
94             peak2 = low1;
95         else
96             flag = 2;
97         end
98     elseif i > low1t && flag == 2
99         if o(i+1) ≥ peak2
100             peak2 = o(i+1);
101             peak2t = i;
102         else
103             flag = 3;
104         end
105     end
106
107 end
108
109 phi_d = p*180/pi;
110
111 % plot results
112 plot(t,tau)
113 title('Transient Response (Load)')
114 xlabel('Time (s)')
115 ylabel('Load (N)')
116
117 figure
118 hold on
119 diff = peak1-(peak1-peak2)/2;
120 mid = diff-(diff-low1)/2;
121 line = 32.25;
122 plot(t,o)
123 plot(t,line)
124 title('Transient Response (Engine Speed)')
125 xlabel('Time (s)')
126 ylabel('Engine Speed (rad/s)')
127
```

```

128 figure
129 plot(t,phi_d)
130 title('Transient Response (Angle)')
131 xlabel('Time (s)')
132 ylabel('Angle ( ^{\circ})')

```

Simulink Model

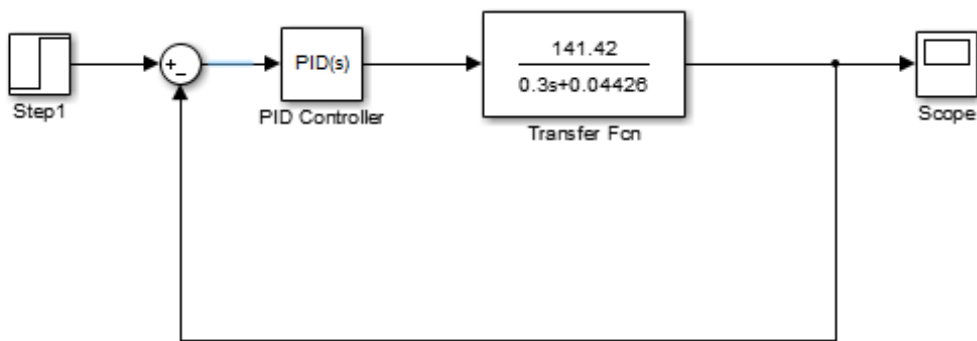


Figure A.9: Simulink Model used to simulate Transient Response of PID Controlled Feedback Loop